4-1-2019

Contact Line Pinning Under AC Electrowetting

Kimberly Bernetski
kab3322@rit.edu

Contact Line Pinning Under AC Electrowetting

By:

Kimberly Bernetski

A thesis submitted in partial fulfillment of
the requirements for the degree of Master of
Science in Mechanical Engineering

Department of Mechanical Engineering
Kate Gleason College of Engineering

Rochester Institute of Technology
Rochester, New York
Submitted April 1st, 2019

Contact Line Pinning Under AC Electrowetting

By:

Kimberly Bernetski

A thesis submitted in partial fulfillment of
the requirements for the degree of Master of
Science in Mechanical Engineering

Department of Mechanical Engineering
Kate Gleason College of Engineering

Approved by:

Dr. Michael Schertzer, Assistant Professor *Thesis Advisor, Department of Mechanical Engineering*	Date
Dr. Kathleen Lamkin-Kennard, Associate Professor *Committee Member, Department of Mechanical Engineering*	Date
Dr. Kara Maki, Assistant Professor *Committee Member, School of Mathematical Sciences*	Date
Dr. Stephen Boedo, Professor *Department Representative, Department of Mechanical Engineering*	Date

ABSTRACT

Sepsis is an autoimmune disease where a bacterial infection causes organ failure. Early diagnosis is a challenge when using traditional methods. Improvement in early detection is vital in treating patients with sepsis. One method for early detection is through the use of particle deposition patterns from patient urine. Deposition patterns are the remaining particles from an evaporating droplet and can vary based on a variety of factors. To optimize sepsis detection, a digital microfluidic device can be used to manipulate the deposition pattern of a sample to detect target proteins. These devices use microarrays for improved biomarker detection. Microarrays consist of arrays of hundreds or even thousands of sessile droplets on a substrate and can be used in several biological applications. These microarrays rely on the application of an electric field to control particle deposition.

Recent efforts have examined the effects of applying electric fields to evaporating droplets to actively control colloidal transport and deposition in evaporating droplets. To improve target protein detection, electrowetting on dielectric (EWOD) is performed to manipulate particle deposition patterns from evaporating droplets. A further understanding of the affects an electric field has on an evaporating droplet would improve device sensitivity. The ability to manipulate the contact line of a droplet is a critical factor in determining fluid dynamics in a droplet. The dynamics of an evaporating droplet ultimately determine the transport and deposition of particles. This thesis focuses on accurately quantifying the forces that affect droplets with and without particles when EWOD. Understanding the forces acting on a droplet will assist in improving manipulating particle deposition patterns. With this goal in mind, the following has been accomplished within this thesis: proposed a new experimentally validated model for hysteresis

under AC electrowetting, verified the proposed model on a variety of different surfaces suitable to EWOD, and performed a preliminary investigation to the effects of particles on hysteresis.

Manufacturing costs limit the availability of many LOC devices as a medical diagnostic tool. Typically, a cleanroom facility with expensive equipment and processing is required to manufacture LOC devices. A potential alternative would be to use an inkjet printer and conductive ink to print electrodes at a much lower cost. These devices could then be coated with a dielectric and hydrophobic layer outside a cleanroom. This thesis verifies if inkjet-printed (IJP) devices are a feasible substitute for cleanroom-fabricated (CRF) devices as EWOD devices.

ACKNOWLEDGEMENTS

First and foremost, I would like to thank my advisor, Dr. Schertzer. If it wasn't for him, I would have never been able to find myself in the field of microfluidics. For the past two years he has provided valuable guidance and insight with the work I have performed within this thesis. He takes a great interest in his students and I am very grateful to have had such an involved advisor. I do not think I would have accomplished as much as I have without his help.

I would also like to thank Dr. Kara Maki, she has always provided additional insight in our biweekly meetings. Her input and encouragement was always greatly appreciated, especially when it came to writing papers.

My lab mates, Collin Burkhart and Heetae An have also provided additional support. Collin helped me when I first joined the lab and ever since has become the best lab buddy anyone could ask for. Heetae assisted with data collection and measurements with some experiments. His input was always valued, and his different perspective helped provide a deeper understanding of material. Additionally, I would like to thank Clayton Terry, Dhanya Thiyagarajan, and Anna Tilstra-Smith for their help the first summer I joined the lab.

I would also like to thank the support of my professors and the department staff in the Mechanical Engineering Department. When I changed my major I was not sure if I made the right choice, but I am very happy I did. The level of diversity of material offered in the department has made me a very well rounded individual. I was provided so many opportunities to learn and grow, not just academically but professionally as well. I know I will be ready to join the job force once I graduate and leave RIT.

I would also like to extend my gratitude towards the College Activities Board, and to my

advisor William St. Jean in particular. I was hired at CAB around the same time I joined the Digital Microfluidics Lab. My role as an event manager has given me invaluable experiences that I could not find elsewhere. It also gave me a chance to expand my horizons and do something unrelated to my work which I think really helped me when it came time to working on this document. My advisor, Bill, has been nothing but patient in answering my questions and helping me grow in my role this past year.

Throughout my five years at RIT, I was able to meet some of the most interesting people who have helped me along the way in some way shape or form. I've known Ray Dodds and Chris Salcedo since first coming to RIT and they have been great friends. In addition, I'd also like to thank Olivier Montmayeur. As a fellow student in the BS/MS program, it was always nice to have someone to sympathize with when equipment failed or something else did not work as expected. It was always nice to know that I was never alone. Finally, I would like to extend my gratitude to Tyler McGrath. Of the people I have met at RIT, he has been the most supportive and I am extremely grateful for his continuous support and motivation.

Lastly, I would like to thank my parents for their continuous support. Without their encouragement I would not have decided to come to RIT to pursue my degree. I am especially grateful to my mother, she has always believed in me and that constant belief and encouragement is what drives me to always give one hundred percent.

TABLE OF CONTENTS

LIST OF FIGURES

LIST OF TABLES

NOMENCLATURE

C	Helmholtz capacitance
C_x	Capacitance of dielectric/hydrophobic layer of device
CD	Contact diameter
CEP	Cyanoethyl pullulan
CRE	Coffee-ring effect
CRF	Cleanroom fabricated
DI	Deionized
DMF	Dimethylformamide
DMFL	Discrete Microfluidics Laboratory
DRLI	Deposition Research Laboratory
d_x	Thickness of dielectric/hydrophobic layer of device
EWOD	Electrowetting on dielectric
ϵ_0	Permittivity of free space
ϵ_{PDMS}	Relative permittivity of PDMS
ϵ_{PTFE}	Relative permittivity of PTFE
ϵ_{SU-8}	Relative permittivity of SU-8
Ew	Electrowetting number
f^0	Unactuated pinning force per unit length
δF	Depinning force
IJP	Inkjet printed

LOC	Lab-on-a-chip
PDMS	Polydimethylsiloxane
POC	Point of care
PS	Polystyrene
PTFE	Polytetrafluorethylene
RMS	Root mean square
θ_0	Apparent initial contact angle
θ^{Ew}	Apparent contact angle due to applied voltage
θ_a	Apparent advancing contact angle
θ_r	Apparent receding contact angle
θ_γ^0	Unactuated equilibrium contact angle
w	Droplet width at interface
U_{RMS}	Applied RMS voltage
γ	Surface tension

1.0 INTRODUCTION

1.1 Background

Sepsis is an autoimmune disease that causes organ failure and death through bacterial infection [1]. In 2011, it was the most expensive condition treated in US hospitals [2]. After decades of research, it remains difficult to treat largely due to challenges associated with early detection. Recent studies found a method of early sepsis detection using patient urine to detect peptidoglycan-associated lipoprotein (Pal) released by *Escherichia coli (E. coli)* [3–5]. Patterns left by evaporating droplets have been used in a variety of medical diagnostic applications [6–9]. Previous work performed immunochemistry in patient samples to determine the presence of target proteins. Using microarrays and fluorescent microscopy, the deposition patterns can be analyzed once the samples evaporate.

Microarrays that manipulate the deposition pattern of a droplet are a subset of lab-on-a-chip (LOC) devices. LOC devices are portable devices that provide quick and inexpensive point of care (POC) testing by combining all processes done in a traditional lab onto one chip. A benefit of LOC devices is the ability to perform POC testing to patients, providing potential life-saving diagnoses to patients. LOC devices can be used to screen for more than just sepsis such as type II diabetes, sexually transmitted diseases, and several cancers [10]. They also have great potential in meeting the World Health Organization's "ASSURED" criteria for ideal rapid test POC devices. To meet the criteria, a device must be (i) affordable, (ii) sensitive, (iii) specific, (iv) user-friendly (simple to perform in a few steps with minimal training), (v) robust and rapid (results available in under 30 minutes), (vi) equipment free, (vii) deliverable to those who need them [11]. Not only do

LOC devices expedite the turnaround time for a diagnosis, they also eliminate expenses such as expensive equipment and well trained technicians [12].

The microarrays used in lab-on-a-chip devices can be used to manipulate and analyze deposition patterns of an evaporating droplet. Deposition patterns from evaporated droplets can be analyzed using fluorescent microscopy in search of target proteins. One proposed method to detect target proteins for sepsis is by using immunoaggregation and dielectric phoretic particle trapping as the sample evaporates. If the target protein is present within the sample, it will clump together due to the immunochemistry and the deposition pattern will appear to be striped (Fig. 1.1). Without the target protein in the sample, the deposition pattern would have a ring deposition.

The transport of particles and colloidal deposition in evaporating droplets is useful for medical diagnostics [7, 11–13] (such as sepsis), fabrication of flexible electronics [14, 15], nanoparticle self-assembly [16–19], containerless materials processing [20], and printing [21]. The "coffee-ring effect" (CRE) is a common deposition pattern [10] which is called as such due to the

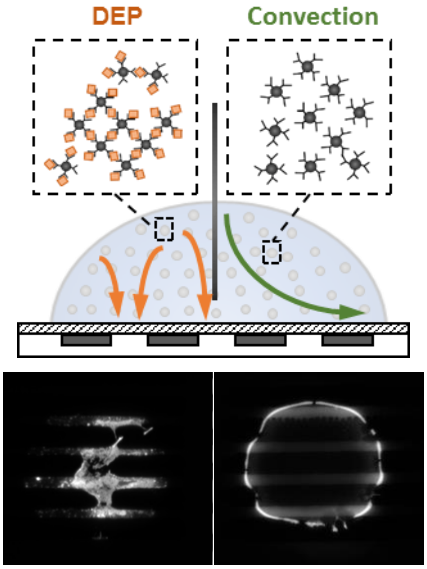

Functionalized particles are introduced to a sample in a droplet as it evaporates

Negative Test (Biomarker not present, right image)
- Evaporative flow drives particles to the contact line by **convection**.
- Result: Ring Deposition.

Positive Test (Biomarker is present, left image)
- Biomarker binds to particle surface.
- Particles bind together and become larger.
- Clumped particles are **steered by DEP and trapped in $+DEP$ or $-DEP$ zones** ($-DEP$ shown).
- Result: Striped deposition.

Figure 1.1 Schematic representation of the operating principle of a proposed proteomic biomarker detection system based on immunoaggregation and dielectrophoretic particle trapping in evaporating droplets.

deposition pattern of the particles after a droplet evaporates. This phenomenon is caused by convective effects, particle diffusion, and boundary effects [22].

Recent investigations have found colloidal deposition can be controlled with AC [23, 24] and DC [25] fields. The evaporative flow of a droplet can be altered by either field type when electrowetting. Investigations have found ring depositions are suppressed with AC fields through improved contact line mobility [26] and electrothermal mixing at frequencies above $\sim 100\ kHz$ [23, 24]. A more uniform deposition results from suppressing ring deposition patterns. Uniform deposition patterns are desirable to improve sepsis biomarker detection.

Another cause of the CRE are pinning forces acting on a droplet at the contact line. These forces prevent the motion of the contact line resulting in the contact angle of an evaporating droplet to decrease (Fig 1.2). A droplet would maintain its shape while decreasing in size without pinning forces. Previous work demonstrates the application of an electric field can affect the pinning force [27]. *Mugele et. al* presents a new model for characterizing the pinning forces when electrowetting on dielectric. This model is compared to experimental data for only one type of device [26].

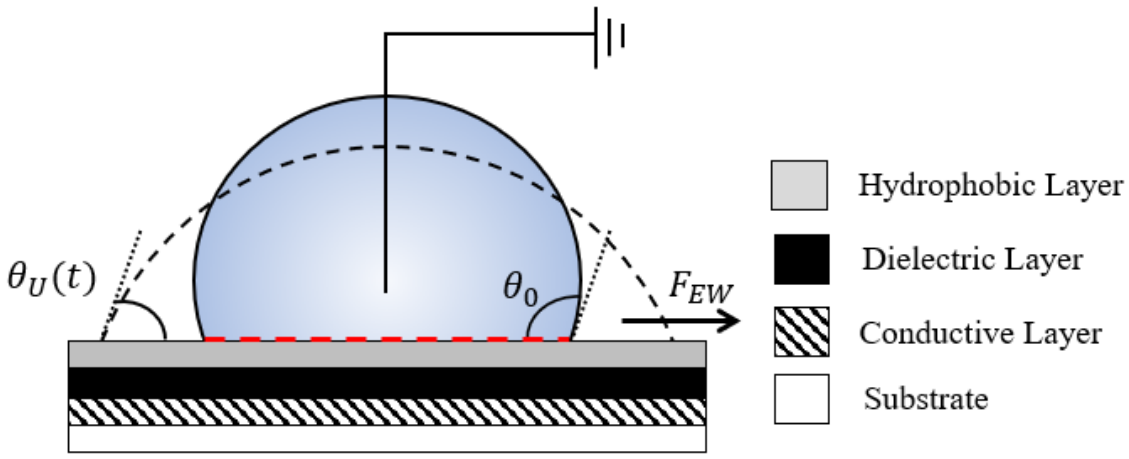

Figure 1.2 Droplet actuated under an electric field. All experiments performed in this thesis follow this setup.

Another study presented in literature observed the addition of particles to a droplet affects the contact line pinning when an unactuated droplet is evaporating [16]. It was observed the addition of particles promotes stick slip behavior.

Difficulties in fabrication are one of the largest reasons LOC devices are not easily implemented. It takes more than 3.5 hours to process [28] a typical experimental device in the cleanroom. This time excludes additional time which is required for the machines to turn on. This is a major inhibitor associated with using a cleanroom due to the significant time required for a machine to reach steady state. Machines can take up to 10 hours to be ready for use. Additionally, one needs a high-end facility with expensive equipment to manufacture an experimental device. The requirements for manufacturing go against the ASSURED criteria.

To meet ASSURED criteria, recent works have begun testing alternative materials such as plastic and paper [29, 30] for microfluidic devices. Similar to *Dixon et. al* [30], this thesis focuses to repeat similar experiments using a relatively inexpensive (~$120) inkjet printer to print metallic ink on chemically treated nano-porous paper. Following printing, these devices are coated with a dielectric and hydrophobic layer without entering a cleanroom. This work differs from *Dixon et. al* [30], largely by the dielectric layer. This proposed solution produces a working device in a fraction of the time at a highly reduced cost.

Inkjet-printed devices (IJPs) are a moderately new means of fabricating microfluidic devices. The Discrete Microfluidics Laboratory (DMFL) at RIT began testing to determine if IJPs are a viable substitute for cleanroom fabricated devices (CRFs). An electric field is applied to these devices to characterize them. Much like Fig. 1.2, a droplet is placed on the hydrophobic layer which is then actuated with an electric field. With a large enough applied force, the pinning forces

that cause the droplet to sit on the surface are overcome. As a result, the contact diameter (dashed red line) increases. The contact angle decreases as the contact line increases.

1.2 Literature Review

1.2.1 Sepsis and Colloidal Depositions for Diagnosis

Sepsis is an autoimmune disease caused by bacterial infection that causes organ failure and death [1]. It was the most expensive condition treated in US hospitals in 2011 [2]. Through decades of research into treatments it remains difficult to treat. Early detection is a major challenge that increases treatment difficulty. Recent studies found one method for early sepsis detection is by using patient urine to detect proteins released by *Escherichia coli (E. coli)* [3]. In 1997 a study discovered IgG in J5 antiserum could bind with three *E. coli* outer membrane proteins: Lpp, OmpA, and peptidoglycan-associated lipoprotein (Pal) [4, 5]. This work focuses on building the stepping stones towards detecting Pal in patient urine through colloidal deposition of evaporating droplets. Microarrays are used to manipulate the deposition pattern of evaporating droplets to create a more uniform deposition. Microarrays are one subset of lab-on-a-chip (LOC) devices which can be used for medical diagnostics.

These devices work by combining all processes done in a traditional lab onto one chip. LOC devices can give potential life-saving diagnoses to patients through quick and inexpensive point of care (POC) testing. Besides, sepsis, LOC devices have potential to screen for type II diabetes, sexually transmitted diseases, and several cancers [10]. They also have great potential in meeting the World Health Organization's "ASSURED" criteria for ideal rapid test POC devices. In order to meet the criteria, a device must be (i) affordable, (ii) sensitive, (iii) specific, (iv) user-friendly (simple to perform in a few steps with minimal training), (v) robust and rapid (results available in under 30 minutes), (vi) equipment free, (vii) deliverable to those who need them [11].

They remove the need for expensive equipment, well trained technicians, and expedite the turnaround time for a diagnosis [12]. There are several types of LOC devices, this thesis focuses on microarray microfluidic devices.

A common technique for processing microarrays is through analyzing deposition patterns using fluorescent microscopy when a droplet dries on the surface [13]. In many cases, a droplet leaves patterns where particles remain in the periphery [31, 32]. The ultimate goal of this research is to design a platform that gives two different types of deposition patterns (Fig. 1.1). One where the target protein is present and one where it is not. If the test results find the biomarker is not present, a ring deposition will result. This is due to evaporative flow driving particles to the contact line through convection. If the results are positive, the deposition will be more uniform. This is due to the biomarker binding to the particle surface and the particles bind together and grow larger. As a result of the clumping of particles, they become trapped on the interface due to their reduced diffusion rate.

To achieve the desired deposition pattern for sepsis detection, a further understanding of the effects an applied electric field has on a droplet is required. The work presented in this thesis isolates the effect of the field on the contact line. A droplet could be manipulated through several different methods besides an electric field. Some of these methods include physical vibrations [23], the use of pumps [7, 8], and applying an electric field [23,33–35]. One method that reports have found to be efficient in droplet manipulation is applying an electric field [36]. Electrowetting on dielectric (EWOD) devices are typically used to manipulate confined [35–38] and unconfined [14, 39-40] droplets. This work focuses on the latter case. An EWOD device consists of an electrode, dielectric layer, hydrophobic layer, and ground electrode Fig 1.2.

1.2.2 Colloidal Transport and Detection

Colloidal deposition of particles in evaporating droplets is useful for medical diagnostics [10,11–13] (such as sepsis), fabrication of flexible electronics [14, 15], nanoparticle self-assembly [16–19], containerless materials processing [20], and printing [21]. Deposition patterns range from coffee-rings to uniform depositions [32, 33]. These patterns are affected by contact line pinning, a high evaporation flux at the contact line [32, 33], and Marangoni recirculation [43] (Fig. 1.3). As a droplet evaporates, Marangoni recirculation carries the particles towards the center of the droplet. This results in a more uniform deposition [43]. Deposition formation can also be affected by Derjaguin, Landau, Verwey, and Overbeek (DLVO) forces which can capture particles on the substrate to form uniform depositions [39]. The DLVO effect is used to examine the net contribution of van der Waals' and electrostatic forces between particles and the surface. When these short-range forces dominate, particles near the substrate can become trapped before being transported to the edge or center of the deposition [39]. In addition to these forces, interface capture, the formation of a skin of particles on a droplet interface, can also affect the deposition patterns [44]. Previous work has found that interface capture occurs when the ratio of interface velocity to particle diffusion rate is greater than the ratio of radial velocity to diffusion rate [44].

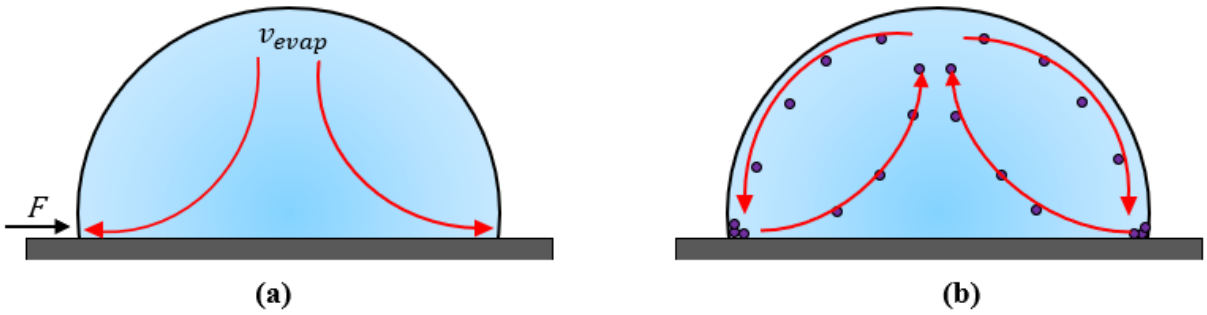

Figure 1.3 Flow of evaporative flux at the contact line of a droplet (a) and flow field of Marangoni recirculation (b).

These factors can be manipulated through EWOD in an evaporating droplet to create more desirable depositions. Sepsis biomarker detection will be improved with a more controlled deposition pattern.

1.2.3 Electrowetting and Its Effect on Transport and Deposition

Devices used within this thesis used various dielectric and hydrophobic layers. When large contact angles are not desired, devices make use of a single polymer film to act as a hybrid dielectric/hydrophobic layer. One way to determine if a material is hydrophobic or hydrophilic is through the initial apparent contact angle θ_0 of a droplet. This is the angle between the solid-liquid interface on a droplet (Fig. 1.4). Layers demonstrating smaller initial contact angles ($\theta_0 \approx 85°$ on SU-8) [28] are considered to be more hydrophilic (Fig. 1.4a). To increase the initial contact angle (Fig. 1.4b) hydrophobic surfaces ($\theta_0 \approx 120°$ on Teflon) are used.

An experimental droplet actuated on Teflon can be seen in Fig. 1.5. The droplet is prevented from experiencing electrolysis (Fig. 1.5b) due to the dielectric layer. Electrolysis is undesirable because it breaks down the device surface and renders areas unusable. This

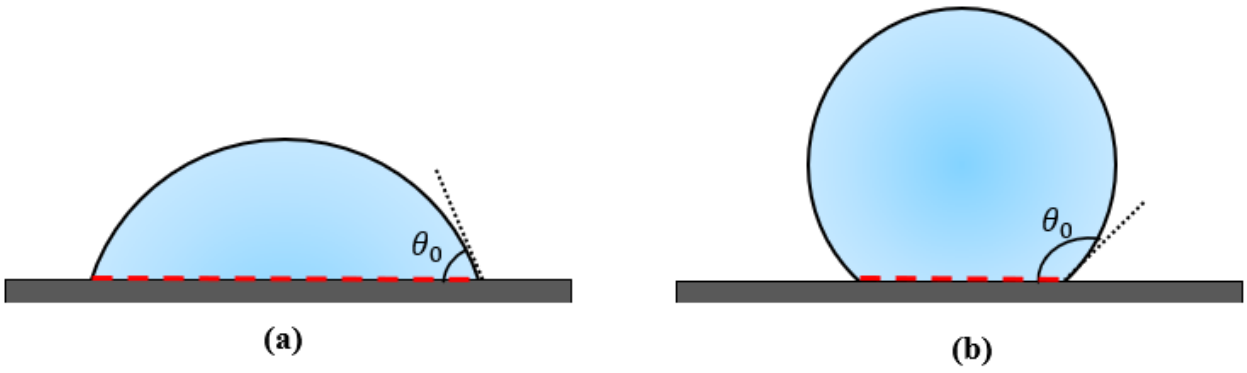

Figure 1.4 Droplet demonstrating a (a) smaller and (b) larger contact angle θ_0. Droplet is on (a) hydrophilic (b) and hydrophobic surface. Dashed red line indicates the contact diameter.

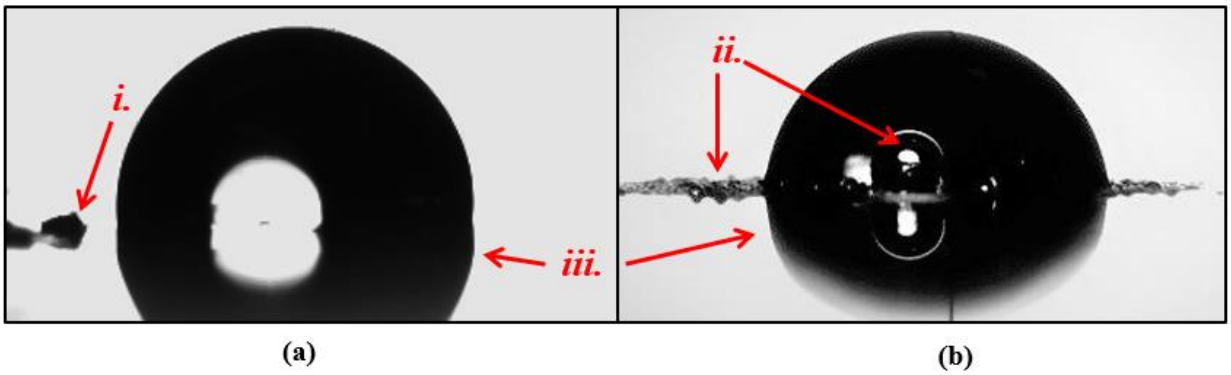

Figure 1.5 Droplet actuated at a lower voltage (a). Actuated droplet experiencing electrolysis (b). Surface inhomogeneity from processing (i), reaction from electrolysis(ii), droplet reflection on electrode (iii).

phenomenon occurs when water is broken into hydrogen and oxygen gas with an electric current. It is observed during actuation when bubbles form within a droplet.

The apparent contact angle of a droplet decreases when a grounded droplet experiences an applied electric field. At lower voltages, this behavior can be described by the electrowetting equation. Derived in 1805, this model focuses purely on the two dimensional geometric surface of a droplet [45]. The terms “contact line”, “contact angle”, and “contact diameter” are introduced to fully understand droplet dynamics (Fig. 1.4). The line where all three phases (surface, droplet, air) meet all the way around the droplet (i.e. circumference of contact) is the contact line. The angle formed between the liquid-gas interface and the liquid-solid surfaces at the contact line is the contact angle. It is measured through the surface. The contact diameter is the intersection between the “two dimensional” droplet and solid interface (respectively) [45]. Between the contact diameter (red dashed line) and liquid-air surface is the apparent initial angle (θ_0). An applied electric field can change the apparent contact angle (θ_{Ew}) (Fig 1.2). This change in angle can accurately be predicted through the electrowetting equation.

The electrowetting equation [10, 23, 34] (Eq 1.1) characterizes how the apparent contact angle changes when EWOD:

$$cos\theta_{Ew} = cos\theta_0 + C_{tot}U_{RMS}^2/2\gamma = cos\theta_0 + Ew \quad (1.1)$$

$$C_x = \epsilon_0\epsilon_x/d_x \quad (1.2)$$

Where θ_{Ew} is the apparent contact angle due to the applied voltage, θ_0 is the initial apparent contact angle, U_{RMS} is the applied root mean squared (RMS) voltage, and γ is the surface tension between the liquid-air interface, and C is the equivalent Helmholtz capacitance of the device. The Helmholtz capacitance of the device can be determined by treating the layers as capacitors in series. The capacitance of each layer can be calculated using Eq. 1.2 where C_x is the capacitance of the layer, ϵ_0 is the permittivity of free space, ϵ_x is the relative permittivity of the material being used for the layer, and d_x is the thickness of the layer. A ratio of electrical and interfacial energies at the solid-liquid interface [35] can be used for non-dimensional analysis. This ratio is referred to as the electrowetting number (Ew). This equation is valid for low to moderate voltages up to a droplet's saturation point. Once the contact angle of a droplet can no longer decrease with increasing voltage, it is saturated.

When the contact angle of an actuated droplet remains constant with increasing voltage it is known to be saturated [47]. Fig 1.6 demonstrates experimental data where an actuated droplet follows the predicted values of the electrowetting equation. Once the droplet reaches saturation $\sim 120\ V$, the

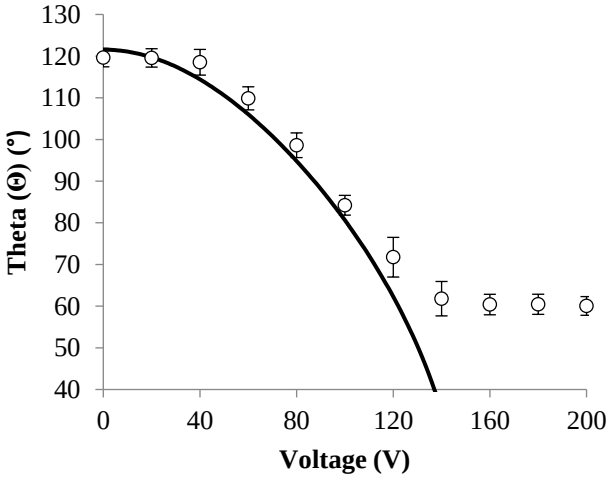

Fig 1.6 Experimental data of actuated droplet using AC voltage (open circles) and electrowetting equation theoretical curve (solid line).

contact angle remains constant with increasing voltage. Some hypotheses why saturation occurs including dielectric breakdown, minimization of electrostatic energy, and contact line instability [47].

1.2.4 Electrowetting and Its Effect on Contact Angle Hysteresis

The pinning force of an actuated droplet could be calculated by examining a balance of the forces per unit length acting on the contact line (Fig. 1.7a). Using the Young equation [46] for an unactuated droplet, the unactuated pinning force per unit length (f^0) is given by,

$$f^0 = \gamma_{SL} - \gamma_{SG} + \gamma_{LG}\cos\theta_0 \tag{1.3}$$

where γ is the surface tension and the subscripts $SL, SG,$ and LG denote properties associated with interfaces between the solid and liquid, solid and gas, and liquid and gas respectively (Fig. 1.7a). For an unactuated droplet, Eq. 1.3 could be manipulated to show

$$f^0/\gamma_{SL} = \cos(\theta^0) - \cos(\theta_Y^0) \tag{1.4}$$

where f^0 is scaled by γ_{SL} and θ_Y^0 is the unactuated equilibrium contact angle. When volume (V) is added to a droplet the contact angle increases from its initial point to a new maximum value,

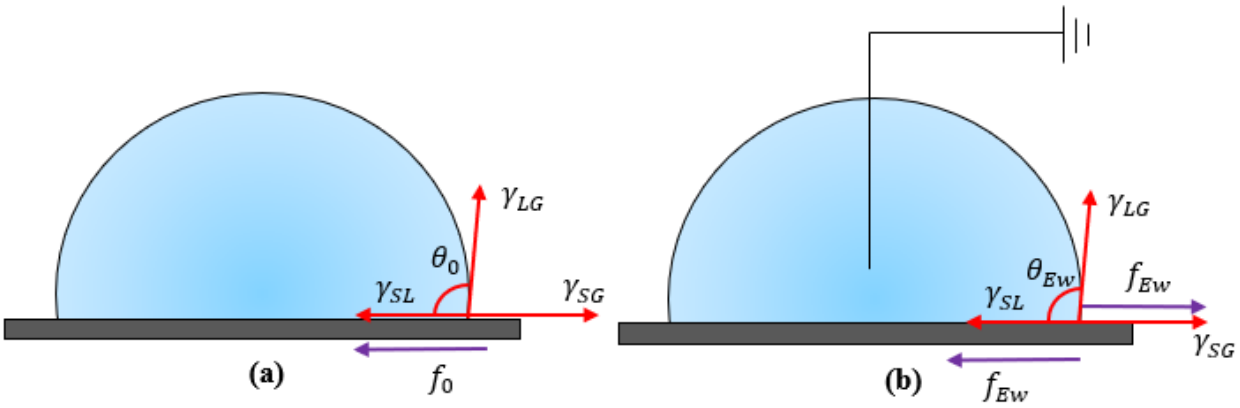

Figure 1.7 The surface tension forces acting in a droplet-substrate system. Sketches show forces per unit length acting on the contact and resultant unbalanced force per unit length in (a) unactuated and (b) actuated cases.

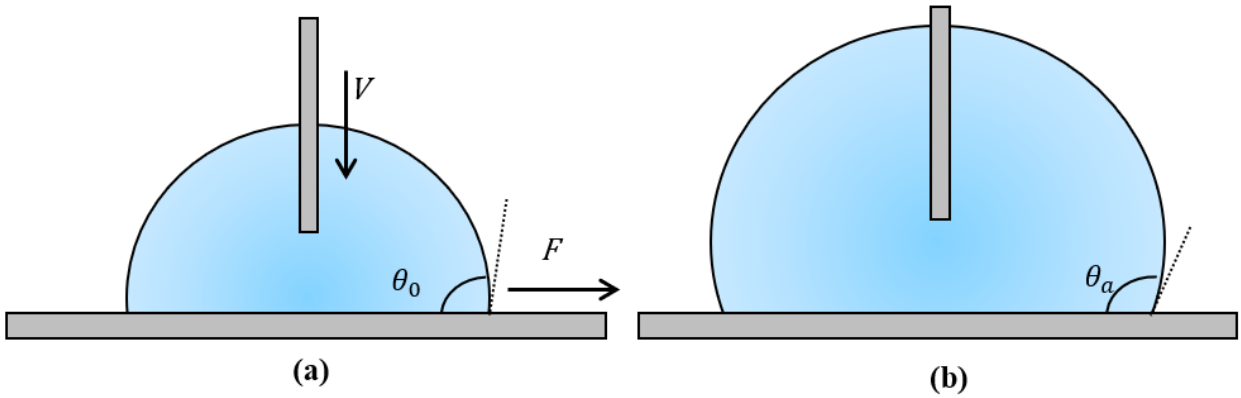

Figure 1.8 Droplet with initial apparent contact angle (a) gaining volume. Resultant apparent contact angle is the advancing contact angle (b).

the advancing contact angle, θ_a (Fig 1.8). Similarly, when the volume is removed, the contact angle reaches a new minimum level, the receding contact angle, θ_r (Fig 1.9) [26]. The difference between the cosine of the advancing and cosine of the receding contact angles can be quantified as the contact angle hysteresis (Fig 1.10). The contact hysteresis value can be used to describe the nondimensional pinning force per unit length. This value is derived using a variation of Young's equation (Eq. 1.3) using the maximum and minimum values at the receding and advancing contact angles, respectively.

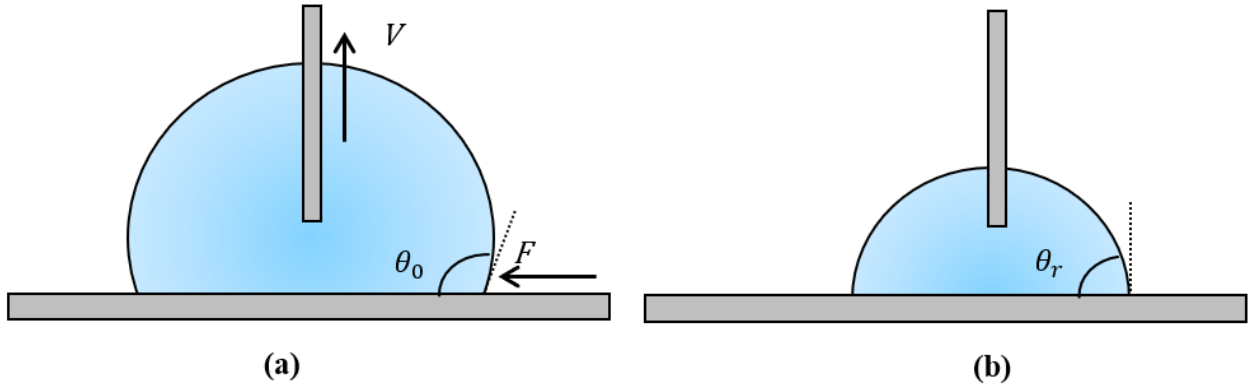

Figure 1.9 Droplet with initial apparent contact angle (a) losing volume. Resultant apparent contact angle is the receding contact angle (b).

$$f_r^0/\gamma_{LM} = \cos(\theta_r^0) - \cos(\theta_Y^0) > 0 \text{ and} \quad (1.5)$$

$$f_a^0/\gamma_{LM} = \cos(\theta_a^0) - \cos(\theta_Y^0) < 0. \quad (1.6)$$

In the previous figures, there is a force F required to overcome the pinning force acting on the droplet. The nondimensional hysteresis value can be used to determine the forces acting on the droplet. These forces that cause a droplet to sit on a surface act similarly to frictional forces. The contact angle at equilibrium can be also affected by chemical heterogeneities and surface defects [14, 38].

To "depin" from equilibrium a droplet must overcome the pinning force (δF) [48]. Much like how an object must overcome some static friction before moving along a surface. Inhomogeneities of the surface are what cause the contact line pinning force to tether the contact line [14, 38]. Understanding how to overcome contact line pinning forces will allow easy manipulation of a droplet's contact line. The contact line pinning force can be quantified by summing Eq. 1.5 and 1.6. As a result the difference between the cosines of the advancing and receding contact angles are used in Eq. 1.7 to find the total pinning forces [26].

$$\delta F_{tot} = \delta F_{advancing} + \delta F_{receding} = \gamma[\cos(\theta_r) - \cos(\theta_a)]. \quad (1.7)$$

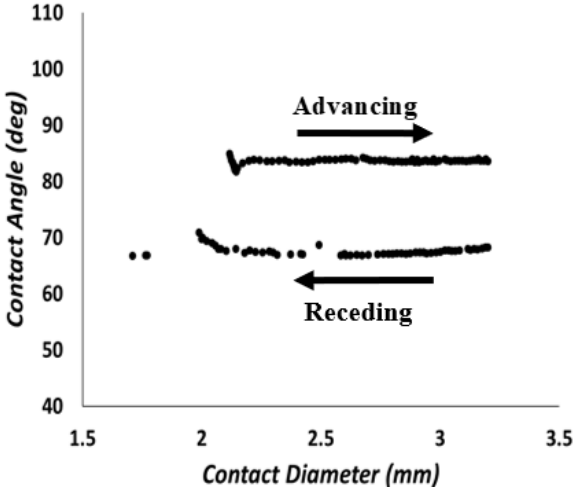

Figure 1.10 Example of raw data used to determine advancing (θ_A) and receding (θ_R) contact angles.

A similar derivation using Young's equation (Eq. 1.3) could be used for an actuated droplet using the electrowetting force (Fig. 1.7b) where

$$f_r^{Ew}/\gamma_{LM} = \cos(\theta_r^{Ew}) - \cos(\theta_Y^0) - f_{Ew}/\gamma_{SL} \text{ and} \tag{1.8}$$

$$f_a^{Ew}/\gamma_{LM} = \cos(\theta_a^{Ew}) - \cos(\theta_Y^0) - f_{Ew}/\gamma_{SL}. \tag{1.9}$$

Mugele et. al [27] analyzed how voltage affects contact angle hysteresis. It was predicted as the voltage increases, contact angle hysteresis decreases linearly, eventually reaching zero with an applied AC signal. The cosine of the receding and advancing angles can be predicted by using Eq. 1.8 and 1.9 to find

$$\cos(\theta_r^{Ew}) = \cos(\theta_r^0) + 0 \text{ and} \tag{1.10}$$

$$\cos(\theta_a^{Ew}) = \cos(\theta_a^0) + 2 \times Ew \tag{1.11}$$

where Eq. 1.10 and 1.11 are only valid up to a critical value when at $Ew_{crit} = (\cos(\theta_r^0) - \cos(\theta_a^0))/2$. Eq. 1.10 implies the receding angle is independent of the applied voltage until Ew_{crit} [27]. Thus, the electrowetting force will help a droplet advance, but not recede. This experiment used four varying voltages, reaching a maximum of $80V_{RMS}$ [27]. It can be seen in Fig. 1.11 the

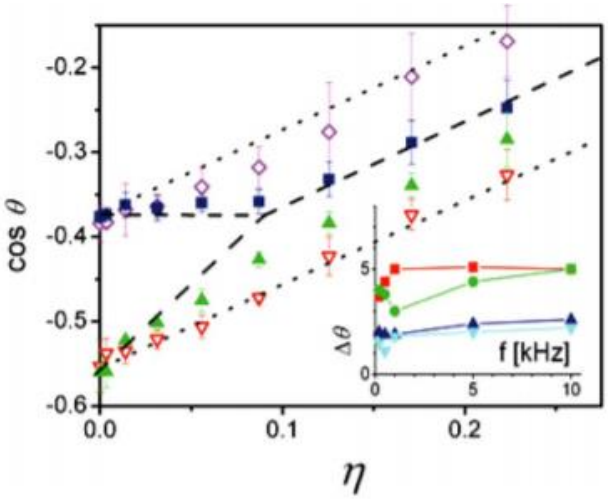

Figure 1.11 *Mugele et. al* advancing (triangles) and receding (squares) experimental data for AC signal (filled) and DC signal (open) as a function of electrowetting ratio (η). Dashed (AC) and dotted (DC) lines predict theoretical values [27].

prediction for AC actuation can be improved in the advancing direction. Further investigation would serve to improve the model. It would also serve to repeat this experiment on a variety of surfaces to determine the validity the model.

Improving sepsis detection requires a further understanding of the effect nanoparticles have on the hysteresis of an actuated droplet. Previous work observed the addition of Titanium (IV) Oxide (TiO_2) nanoparticles promotes stick-slip behavior [49]. This work observed the contact line pinning due to the accumulation of nanoparticles at the contact line and not surface defects. The effects of TiO_2 nanoparticles in various concentrations was quantified for an unactuated evaporating droplet [49]. The work performed in this thesis would serve to further examine how nanoparticles affect the contact line when a droplet is actuated. Literature suggests there has not been any analysis performed on the hysteresis of droplets with nanoparticles under the influence of an electric field.

1.2.5 Accessibility/Fabrication of EWOD Devices

Another goal of this research was to determine if there is a viable fabrication method for devices that will meet ASSURED criteria. Inkjet-printed (IJP) devices require less time and equipment to manufacture which meets part of the ASSURED criteria. This research determines the validity of substituting IJP devices for CRF devices. The main goal is to discover if there is a difference in the pinning forces between devices. *Dixon et. al* investigated the use of an Epson Stylus C88+ inkjet printer for electrode fabrication [30]. Printed devices used cyanoresin CR-S cyanoethyl pullulan (CEP) as the dielectric material due to its optimal electrical properties. The dielectric constant of CEP is approximately 18 [50] at room temperature while SU-8 3005 is approximately 3.28 [51]. To create a sufficient dielectric layer, CEP must be diluted using an organic solvent, dimethylformamide DMF [52]. DMF is a very flammable and toxic chemical

which requires the use of a specialized laboratory for processing. ASSURED criteria will not be met with the additional requirement for specialized equipment. Devices must meet ASSURED criteria to make device production more feasible and easily implemented commercially. Work performed in this thesis repeats IJP device fabrication similar to what has previously been done with a safer chemical as the dielectric layer.

1.3 List of Contributions

This investigation is to further understand and quantify the effects electrowetting on dielectric has on the pinning forces of a droplet. To simplify analysis, experimentation is broken up into three different phases: electrode manufacturing, hydrophobic surface type, and presence of particles. As a result, this work makes four primary contributions.

1. Verify the validity of using IJP devices as a substitute for CRF devices. A methodology for manufacturing these devices was also determined.
2. Investigate the existing model proposed by *Mugele et. al* [27] to predict the advancing and receding angles of a droplet. This model has been updated to more accurately predict the advancing and receding angles at low to moderate voltages.
3. Verify updated model for predicting the advancing and receding angle of actuated droplets on several types of surfaces.
4. Investigate the effects the presence of nanoparticles have on the hysteresis of an actuated droplet. Measurements were compared with updated hysteresis model.

This work has been published in the following:

1) K.A. Bernetski, C.T. Burkhart, K.L. Maki, M.J. Schertzer, Characterization of electrowetting, contact angle hysteresis, and adhesion on digital microfluidic devices with inkjet-printed electrodes, Microfluid. Nanofluidics. 22 (2018) 1–10.
2) K.A. Bernetski, K.L. Maki, M.J. Schertzer, Comment on “How to make sticky surfaces slippery: Contact angle hysteresis in electrowetting with alternating voltage” [Appl. Phys. Lett. **92**, 244108 (2008)], Appl. Phys. Lett. 114 (2019) 116101.

The following work is also in preparation:

3) K.A. Bernetski, K.L. Maki, M.J. Schertzer, (In preparation) A model for contact angle hysteresis under AC Electrowetting on a variety of surfaces.

All necessary data for the initial submission of this paper is presented here and submission to Applied Physics Letters is expected by May 2019.

2.0 RESEARCH QUESTION

The following question is the primary goal of this thesis: **How are contact line pinning forces affected by electrowetting?** This question can be broken up into the following four components:

1. **How does electrowetting affect contact line pinning in particle free droplets?**

Literature suggests contact line pinning forces can be quantified through the apparent advancing and receding contact angle [27]. The apparent initial contact angle is dependent on the top layer of microfluidic devices. Observing the amount of force required to overcome different apparent contact angles would provide insight on the current model used to quantify contact line pinning forces. Results will be compared to data presented in literature [27].

2. **Does the type of hydrophobic surface affect contact line pinning forces?**

The updated model presented in [53] is tested on several devices with varying hydrophobic layers using similar procedures outlined in [27]. This verifies the validity of this model over a variety of types of surfaces with different material properties.

3. **Do variations in the electrode manufacturing process affect the contact line pinning forces?**

Two variations to the manufacturing process will be used for this research. Comparisons between IJP and CRF devices will be observed to discern if the type of electrode affects a droplet's ability to overcome the pinning forces. Experimentation in this thesis also provides insight on the reliability of IJP devices as a viable substitute for DMF devices.

4. How does particle concentration affect contact line pinning forces?

One key aspect to improving sepsis detection is understanding the characteristics of droplets with different concentrations. Experimentation involved similar tests as the previous two questions with DI droplets using $22nm$ polystyrene (PS) particles at various concentrations.

3.0 EXPERIMENTAL METHODOLOGY

The five components of the experimental facility used in this investigation are outlined in this chapter. The methods for creating the droplets and devices are explained in addition to a list of the equipment for data collection. The general setup for all experimentation is presented in Fig. 1.2.

3.1 Droplets

All droplets for research questions two and three are deionized (DI) water purchased from Sigma Aldrich. Research question four required the use of $22nm$ polystyrene (PS) particles within the droplets. Deionized water was used as the solvent for all droplets with particle concentrations of 0.001% and 0.01%.

All experiments performed in this thesis followed one of two procedures for depositing droplets. For the first case, all droplets were deposited on the substrate using an Ependorf Research Plus micropipette. Droplet volumes for static experiments were $3\mu L$ for all experiments. Uncertainty in volume of deposited droplet is reported to be +/- 3% by the manufacturer. In the second case, droplets were deposited using a Rame-Hart Auto Dispensing unit. Fluid was added and removed from droplets at a constant rate of $0.17\ \mu L/s$ and $0.25\ \mu L/s$ respectively.

3.2 Devices

Table 3.1 Inkjet Printer Settings

Parameter	Setting
Quality	Best Photo
Paper	Ultra Glossy
Print	High Speed Off

Two types of devices were fabricated for experimentation. Coating for dielectric and hydrophobic layers followed similar procedures for both devices. Devices differed through the bottom substrate and method for electrode deposition. Most experiments used glass slides with Aluminum deposited

purchased from Sigma Aldrich. For this thesis, these devices will be referred to as cleanroom fabricated (CRF). Research question three also used inkjet printed (IJP) devices where the electrode was deposited using an Epson C88+ Color Inkjet printer. Electrode deposition on these devices followed similar procedures as the literature [30].

Similar to [30], ink cartridges were filled with Novacentrix JS-B25P silver nanoink purchased from Novacentrix. The printing medium was Novacentrix Novele, a nanoporous and chemically treated photopaper. The print settings used can be found in Table 3.1. After several trials it was observed the printer was more effective with low resolution prints. The highest resolution observed was $100\ nm$ for line thickness and $200\ nm$ for line spacing. A more complex design (Fig. 3.1a) has higher potential to have unwanted connections that could result in a short circuit. All electrodes used within this thesis do not require any resolution greater than Fig. 3.1b.

Following printing, the IJP device must be coated with a dielectric and hydrophobic layer. Using a Laurell spin coater (WS-650-23), thin films were deposited then baked on a Fisher Scientific Isotemp hotplate. The methodology used to deposit these thin films were the same between IJP and CRF devices to reduce variability. Three types of materials were used as the

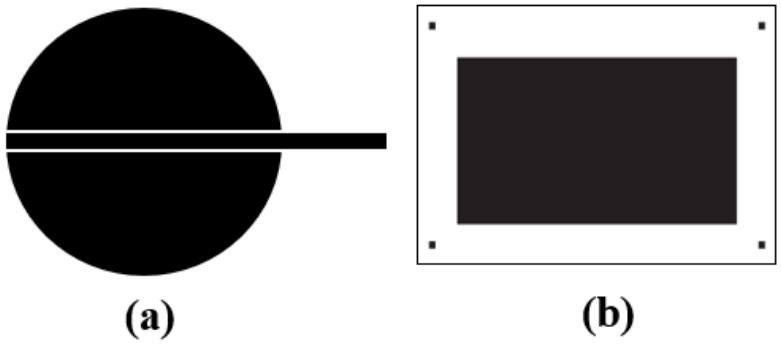

Figure 3.1 A section of a more complex design that requires higher printer resolution (a). A simple design that requires very low resolution from printer (b). All work performed in this thesis did not exceed complexity of (b).

hydrophobic or dielectric layer throughout this thesis.

Dielectric films varied between PDMS and SU-8 3005. To obtain a dielectric thickness of $\sim 10.5\ nm$ PDMS was deposited using a two-stage spin coating process ($500\ rpm/s$ ramp-up for $5\ s$; $6000\ rpm$ for $30\ s$ with $1000\ rpm/s$ between stages). Devices can remain on spin coater at $6000\ rpm$ for a longer period of time to reduce dielectric thickness. Devices are then hard baked using a Fisher Scientific Isotemp hotplate at $95\ °C$ for 15 minutes. Devices coated with PDMS used the thin film as both the dielectric and hydrophobic layer.

Deposition of SU-8 followed a similar procedure. SU-8 was deposited to obtain a dielectric thickness of $\sim 6.5\ \mu m$. Films were deposited using a two-stage spin coating process ($500\ rpm$ for $10\ s$; $4000\ rpm$ for $30\ s$; $300\ rpm/s$ between stages). Devices were then soft baked at $95\ °C$ for two and a half minutes, cured in an Electro-Lite EC-500 ($365\ nm$ for $30\ s$), and hard baked at $150\ °C$ for three minutes. Some SU-8 devices would have an additional thin film deposited to act as the hydrophobic layer. Teflon (PTFE Teflon AF $\sim 100\ nm$) layers were deposited on the dielectric layer. Films were spun onto devices for one minute at $2000\ rpm$ then hard baked for ten minutes at $160\ °C$.

It was found that the print media used for IJP devices appeared to react with the SU-8 film

(a) (b)

Figure 3.2 Electrode after processing with SU-8 as first layer on Novacentrix Novele paper (a). Electrode after processing with Teflon as first layer on Novacentrix Novele paper (b).

(Fig. 3.2a). Breakdown of droplets occurred at voltages as low as $40\ V_{RMS}$ on these devices as well. To remedy this issue, a $\sim 100\ nm$ film of Teflon was deposited as a base layer on all IJPs (Fig. 3.2b). This bottom layer acts as a barrier between the SU-8 and print media in addition to electrolysis at low voltages.

3.3 Profile Imaging

Droplet profiles were imaged using a Ramè-Hart model 250 goniometry system (Fig. 3.3a). Devices are positioned on the stage where droplets are then deposited (Fig. 3.3b). The imaging system consists of a CCD camera (659x494 pixels) and a backlit 5-axis stage. Prior to each set of experiments the system is leveled and calibrated. Side view images are recorded of the droplet at rates ranging between one tenth to one frame per second (fps).

Ramè-Hart DROPimage Advanced software is used to analyze images taken during experiments. Droplets are detected through the program and optically calculates the droplet's maximum width and contact angle. The width and mean contact angle are used to calculate the

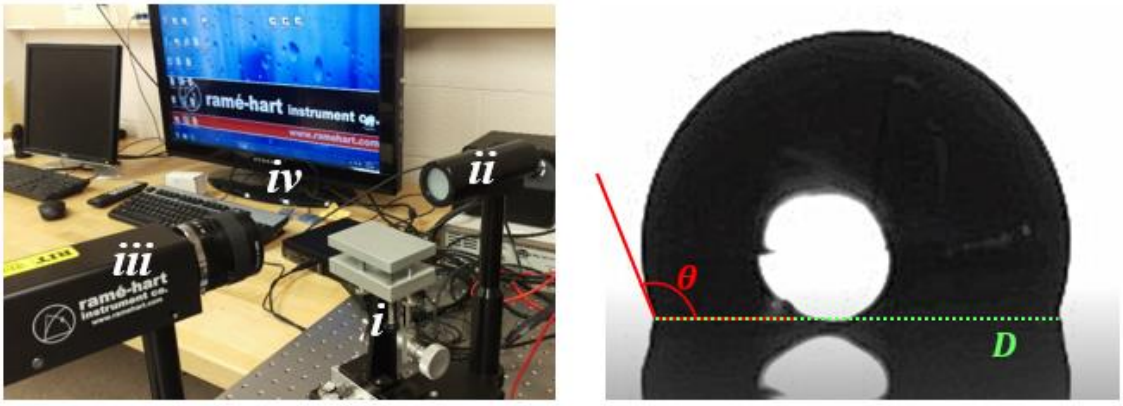

Figure 3.3 Ramè-Hart experimental setup (a) where device is placed on stage (i), illuminated by back-light (ii), imaged using camera (iii), and observed using monitor (iv). Droplet imaged using experimental setup where the contact angle and contact diameter can be measured and calculated (b).

contact diameter,

$$CD = w * \sin(\theta_U) \tag{3.1}$$

where CD is the calculated contact diameter and w is the width of the droplet at the interface. This measurement is only valid when a droplet's contact angle is larger than 90°. The software calculates the left and right contact angle of the droplet and calculates the resulting mean of the droplet which is used for analysis.

A backlight is used to provide further contrast between the droplet and background. The droplet must also be focused with crisp edges. The starker the contrast and crisper the image, the easier it is for the software to detect the droplet area. The backlight causes the white spot in the center of the droplet in Fig. 3.3b which can lead to measurement errors. Prior to running the experiment, an area can be defined to exclude any calculations. The user places two lines at the right and left outer edge of the white spot to define the area (Fig. 3.4). The device also causes the droplet to display a reflection which also can affect measurements. A baseline is defined where the droplet is resting on the device to exclude the reflected area (Fig. 3.4). Throughout the

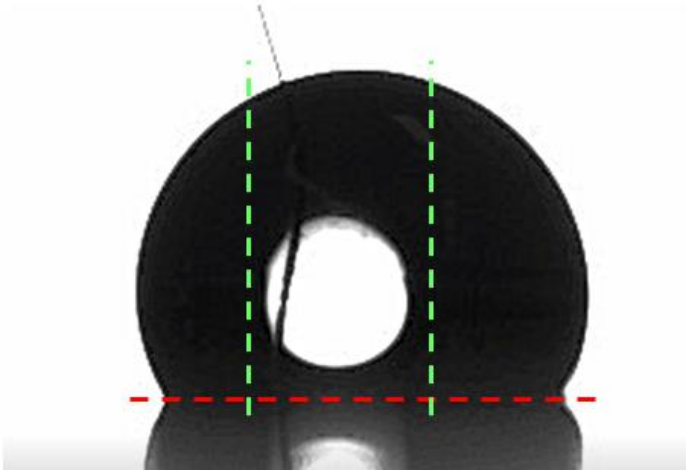

Figure 3.4 Imaged droplet where baseline is defined (red dashed). Area ignored during measurements (between green dashed).

experiment the program creates a log file of the contact angle and maximum contact width which can be imported into Excel for analysis.

3.4 Depositing Droplets

Droplets were placed on the substrate using two methods. Electrowetting experiments used deionized (DI) water. Using a micropipette, $3\mu L$ droplets were placed onto the substrates prior to adding the ground wire. Contact angle hysteresis experiments required volume to be added and removed from droplets at a constant rate. A Ramé-Hart Automated Dispensing System was used to add and remove fluid at a constant rate of $0.17\ \mu L/s$ and $0.25\ \mu L/s$, respectively.

3.5 Actuation

Droplets were actuated using both an AC and DC signal produced by an NI PXI-5402 signal generator. All experiments that required AC frequency were actuated with a $1\ kHz$ frequency. Droplets were actuated at a range of voltages, reaching a maximum of $260\ V_{RMS}$. The signal was applied to the bond pad on the device and continuously monitored using an NI PXI-4072 digital multimeter. Droplets were grounded by inserting a $22\ nm$ diameter tungsten wire in the center of the droplet.

4.0 RESULTS AND DISCUSSION

Pinning forces cause a droplet to maintain its shape on a surface by preventing motion of the contact line. These forces are what affects an evaporating droplet's contact angle to decrease when the contact line is effectively pinned. Without pinning forces, an evaporating droplet would continue to decrease in size while maintaining the same shape. If the contact angle of a droplet is not manipulated, particles will deposit themselves around the contact line in a pattern commonly known as the "coffee-ring effect" (CRE) [54]. One common way to suppress the CRE in microfluidic devices is through electrowetting on dielectric (EWOD). Further understanding the effects pinning forces have on deposition patterns; for instance, the CRE when EWOD, further improvements to applications such as printing, biochemical analysis, and manufacturing of nano-structured materials through colloidal and macromolecular patterning, can be made [54].

Pinning forces are commonly quantified through the contact angle hysteresis. The difference between the advancing and receding apparent contact angles describes contact angle hysteresis. The advancing angle can be measured as the apparent contact angle as fluid is being added to a droplet. Similarly, the receding angle is the apparent contact angle as fluid is removed from a droplet [27]. The total dimensionless pinning force acting on the droplet can be described by the difference between the cosine of the advancing and cosine of the receding angles. This method of quantifying the pinning forces is valid for any electrowetting value.

This work focuses on the different factors that have the potential to affect the contact line forces when EWOD. The four main factors this thesis focuses on includes: effect electrowetting has on contact line pinning, top surface type, electrode manufacturing, and particle concentration in the droplet. Experiments follow two types of tests: electrowetting to test validity of devices with

electrowetting equation (Eq. 1.1) and hysteresis. All devices used within this thesis are basic unpatterned electrodes and unless specified otherwise, CRF devices.

4.1 Electrowetting Effect on Contact Line Pinning

As previously stated in Section 1.2.4, the model used to predict the advancing and receding contact angles of an actuated droplet can be improved. Analyzing the model presented in [27], Eq. 1.10 and 1.11 are derived from the transient dimensionless electrowetting force for sinusoidal waveforms given by

$$\frac{f^{Ew}(t)}{\gamma_{LM}} = \frac{CU_{pk}^2}{\gamma_{LM}}\sin^2(\omega t) = \frac{CU_{rms}^2}{\gamma_{LM}}[1-\cos(2\omega t)] = Ew[1-\cos(2\omega t)], \tag{4.1}$$

where $f^{Ew}(t)$ is the electrowetting force per unit length at a given electrowetting number and time t, U_{pk} is the peak voltage, and ω is the actuation frequency. Eq. 1.10 and 1.11 are characterized through the minimum and maximum values of Eq. 4.1.

While the maximum electrowetting force more accurately predicts actuated advancing contact angles than the time averaged value for AC signals, published data on Teflon suggests it still underpredicts actuated advancing contact angles for an applied AC signal (Fig. 4.1). If the RMS value of the electrowetting force from Eq. 4.1 is used, it provides a more accurate prediction for the advancing contact angle. Using the RMS value of the electrowetting force is hypothesized to capture the transient nature of the term, while implying the contact line motion is not dominated by the instantaneous maximum. Since the RMS value of Eq. 4.1 is $\sqrt{3/2} \times Ew$, the model for the advancing angle under AC signal replaces Eq. 1.11 with

$$\cos(\theta_a^{Ew}) = \cos(\theta_a^0) + \sqrt{3/2} \times Ew. \tag{4.2}$$

Using the RMS electrowetting force for the advancing angle is similar to choosing the RMS voltage to describe the apparent contact angle when electrowetting.

Another update to the model proposed by *Mugele et. al* [27] assumes that θ_r^{Ew} and θ_a^{Ew} are bounded by the electrowetting equation [55] (Eq. 1.1). This replaces the assumption that the advancing and receding angle follow Eq. 1.10 and 1.11 until they converge at some critical electrowetting number (Fig. 4.1). While their model deviated from this prediction (Fig. 1.11), it was attributed to several effects including: depinning being a transient process, the electrowetting force being distributed over a distance equal to the thickness of the dielectric layer, and variability in contact angle data at high electrowetting numbers [27].

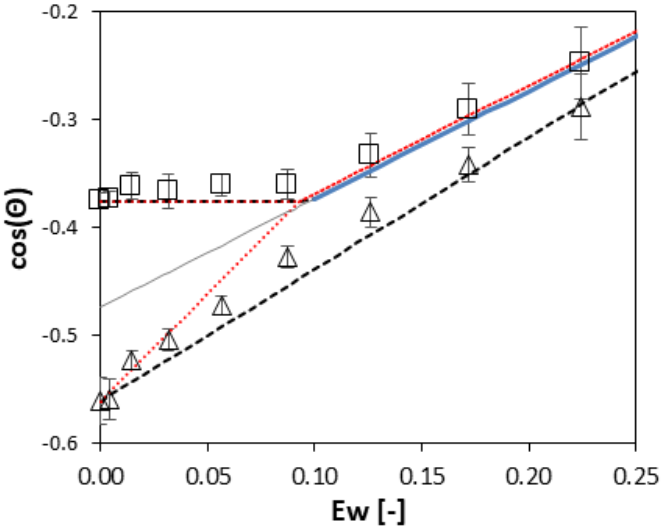

Figure 4.1 Cosines of advancing (triangles) and receding (squares) data on Teflon device [27]. Previous prediction for advancing and receding data (red dotted) and updated prediction for advancing and receding data (black dash), and the electrowetting equation before (solid gray) and after (solid blue) intersection with the proposed prediction for cosine of the receding contact angle.

Fig. 4.1 presents data from [27] comparing both models. The updated model more accurately describes the pinning forces acting on actuated droplets on Teflon devices. This work has been submitted and accepted as a comment in the Applied Physics Letters [53].

4.2 Surface Type

After verifying the proposed model improved hysteresis predictions on Teflon based on measurements published in [27], devices with varying initial contact angles were tested to verify the model works on a variety of devices. Teflon ($\theta_0 \approx 120°$), PDMS ($\theta_0 \approx 120°$), and SU-8 3005 ($\theta_0 \approx 85°$) were selected due to their varying initial contact angles and material properties. Devices

that used Teflon as the hydrophobic layer also had a layer of SU-8 to act as the dielectric. Devices with PDMS and SU-8 used the material as both the dielectric and hydrophobic layer. Electrodes for these devices were purchased through the Deposition Research Laboratory, Inc. (DRLI). Dielectric and hydrophobic layers were deposited in the Material Science Laboratory at RIT. The layer deposition process is outlined in Section 3.2.

Device performance is analyzed using Ew, and not applied voltage (U_{RMS}), due to a variance in the capacitance per unit area between devices used within this investigation. This variance is due to the electric permittivity and total layer thickness of the hydrophobic and hydrophilic devices. Electrowetting numbers on all device types were determined through Eq. 1.2 using the following parameters: the surface tension between the droplet and surrounding air ($\gamma = 72.8\, mN/m$), the permittivity of free space ($\epsilon_0 = 8.85\, pF/m$), and the relative permittivity of SU-8 ($\epsilon_{SU-8} = 3.2\ [-]$), PTFE ($\epsilon_{PTFE} = 2.0\ [-]$), and PDMS ($\epsilon_{PDMS} = 2.5\ [-]$).

Two types of experiments were performed on these devices. The first test was designed to ensure all devices functioned correctly through analysis of electrowetting performance. Electrowetting performance was analyzed by measuring the apparent contact angle as a function of applied voltage. Deionized (DI) water droplets ($3\ \mu L$) were deposited on the large unpatterned conductive layer for each device type using a micropipette prior to grounding with a $22\, nm$ tungsten wire. All devices were actuated using a $1\ kHz$ AC signal. Actuation ranged between $0 - 260\ V_{RMS}$ in $10 - 20\ V$ increments. Droplets remained at a constant voltage for a minimum of 5 seconds before the voltage increased. To eliminate any effects of fouling of the surface, measurement sites were never reused from test to test. Devices were placed on the backlit stage of a Ramé-Hart model 250 goniometer to capture side-view images at a rate of 10 frames per second (fps). For each frame, DROPimage Advanced software was used to measure the droplet width and

mean contact angle.

Electrowetting performance for all three devices was well predicted up to saturation by Eq. 1.1. Deviation from the prediction occurs at similar Ew on Teflon ($U \approx 120\, V_{RMS}, Ew \approx 0.60$), PDMS ($U \approx 200\, V_{RMS}, Ew \approx 0.60$), and SU-8 ($U \approx 120\, V_{RMS}, Ew \approx 0.50$). The difference between devices in Fig. 4.2 is expected due to the varying dielectric layer thickness as well as initial apparent contact angle. The higher initial contact angle on PDMS and Teflon devices led to a more rapid decrease in apparent contact angle as applied voltage (or electrowetting number) increased. The PDMS device required a higher voltage to reach saturation due to a thicker dielectric layer. This was expected due to the electrowetting equation. The larger uncertainty seen in the SU-8 device is due to the variation in the initial contact angle. This could be due to a varying dielectric thickness throughout the device from the spin coating procedure.

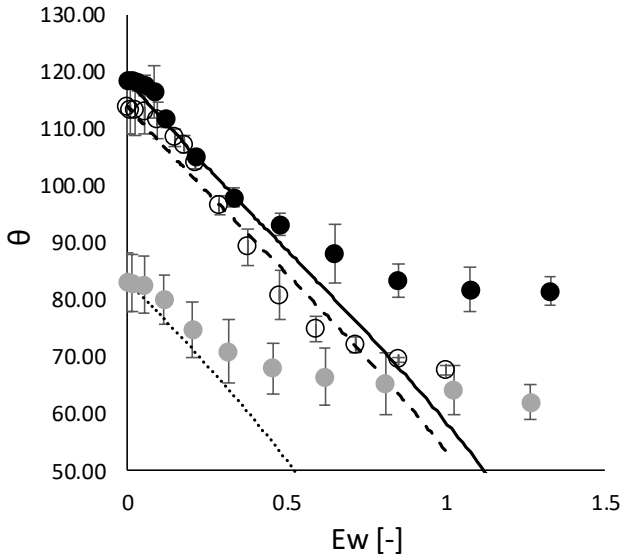

Figure 4.2 Experimentally observed apparent contact angles on Teflon (black), PDMS (open), and SU-8 (grey) devices as a function of AC voltage. Solid, dashed, and dotted lines represent predictions from electrowetting equation (Eq. 1.1)

The second set of experiments utilized a similar procedure to measure the contact angle hysteresis as a function of applied voltage. The purpose of these experiments was to determine how well Eq. 1.10 and 1.11 from [27] predict the cosine of the advancing and receding apparent contact angles. A Ramé-Hart Automated Dispensing System was used to add and remove fluid from a droplet at a constant rate of ~0.17 $\mu L/s$ and ~0.25 $\mu L/s$, respectively.

The first set of hysteresis experiments performed were on Teflon devices (Fig. 4.3). The red dotted lines represent the predicted advancing and receding values as a function of the electrowetting number through Eq. 1.10 and 1.11. This model predicts the advancing and receding contact angle well, more accurately for receding angles. While this model may be adequate to predict the advancing and receding apparent contact angle for devices with Teflon as the top layer, there is a higher level of uncertainty for PDMS and SU-8. PDMS (Fig. 4.4) and SU-8 (Fig. 4.5) devices were not well predicted through Eq. 1.11 for the advancing angle. It can also be observed the advancing and receding values do not intersect at $Ew_{crit} = (\cos(\theta_r^0) - \cos(\theta_a^0))/2$ as predicted by [27] for any case. The updated model proposed in the previous

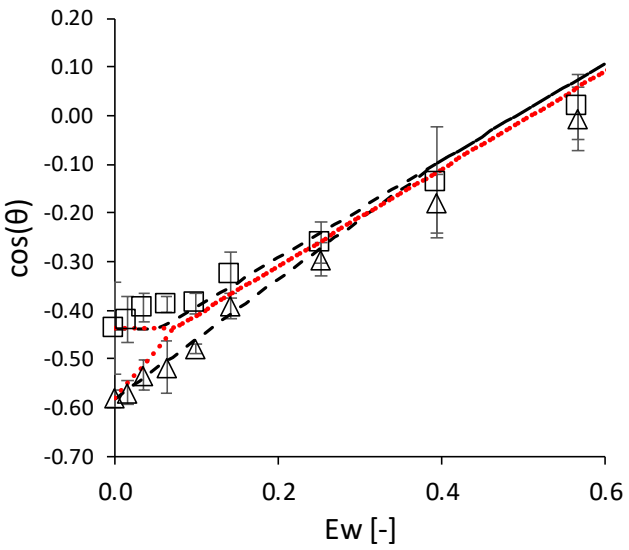

Figure 4.3 Experimentally observed advancing (triangles) and receding (squares) contact angles as a function of *Ew* on Teflon devices. Red dotted (*Mugele et. al*) and black dashed (proposed) lines predict the contact angles.

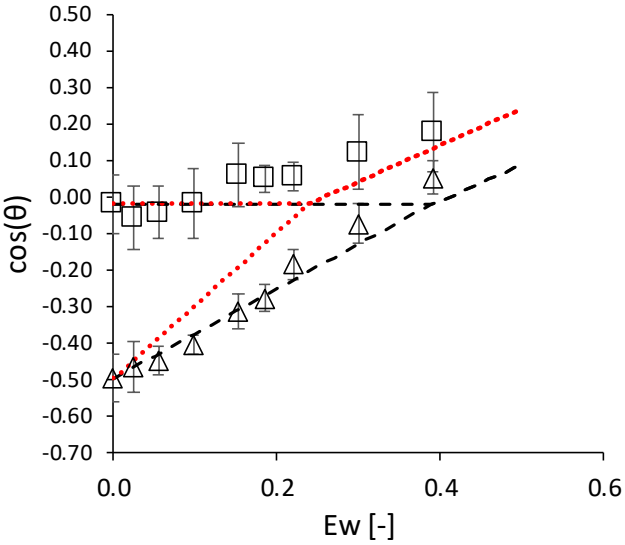

Figure 4.4 Experimentally observed advancing (triangles) and receding (squares) contact angles as a function of *Ew* on PDMS devices. Red dotted (*Mugele et. al*) and black dashed (proposed) lines predict the contact angles.

section is compared against the model from [27] in Fig. 4.3-4.5.

With these two updates to the model, the advancing and receding data is more accurately characterized for all three types of devices (Fig. 4.3-4.5). As the electrowetting value increases so does the level of uncertainty of the model. The uncertainty of the data could potentially be due to the device reaching saturation. The uncertainty in the receding data could potentially be due to liquid sorption or solid swelling [56]. This affects the reproducibility in experimental receding data.

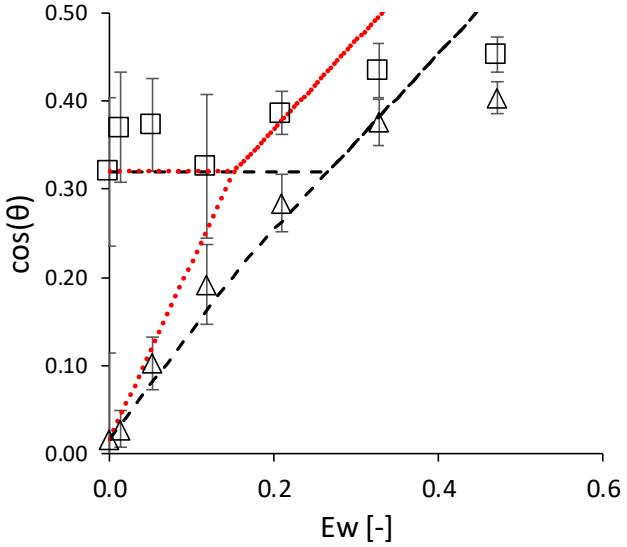

Figure 4.5 Experimentally observed advancing (triangles) and receding (squares) contact angles as a function of *Ew* on SU-8 devices. Red dotted (*Mugele et. al*) and black dashed (proposed) lines predict the contact angles.

This updated model only predicts the advancing and receding contact angles at low to moderate voltages. It is 20%, 60%, and 55% more accurate for low to moderate voltages on Teflon, PDMS, and SU-8 (respectively). Similar to the electrowetting equation, once the apparent contact angles reach a threshold, the angles become saturated. As a result, the hysteresis never fully reaches zero as predicted [27]. This is potentially due to the roughness of the surface. The variation in the saturated hysteresis values between devices could be attributed to the differing material properties of the devices.

4.3 Manufacturing Method

Two forms of electrode fabrication were implemented within this thesis. The cleanroom fabricated (CRF) device used a plain electrode which was fabricated in the Semiconductor and Microsystems Fabrication Laboratory (SMFL) at RIT. This device had a layer of SU-8 as the dielectric layer and Teflon as the hydrophobic layer (Fig. 4.6a). The second device type was made completely outside the cleanroom using an Epson Stylus C88+ inkjet printer. The inkjet printed (IJP) devices were later spin coated in the Biomaterials and Assistive Device Laboratory at RIT. The IJP devices required a "buffer" layer (Fig. 4.6b) of Teflon between the electrode and SU-8 to prevent the SU-8 from reacting with the Novacentrix Novele print media. Device manufacturing followed the procedures outlined in Section 3.2. Electrodes did not require a high level of resolution for this work. The design for electrodes remained simple (Fig. 3.1b).

Experimentation followed similar procedures outlined in Section 4.2. Comparison between IJP and CRF devices utilized the electrowetting equation and hysteresis experimentation. The first experiment was designed to determine if both devices followed electrowetting equation. Droplets of deionized (DI) water with a volume of 3 μL were placed on the electrode demonstrated in Fig.

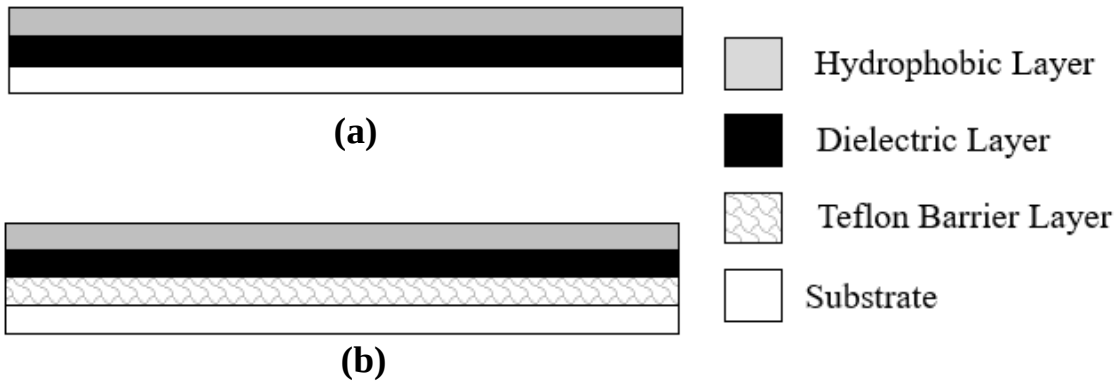

Figure 4.6 Layers of CRF (a) and IJP (b) devices used for experimentation.

1.2. Experiments actuated droplets at varying DC and AC voltages ranging between $0 - 200\ V_{RMS}$ in $20\ V$ increments and at a frequency of $1\ kHz$ for the AC case. This procedure was run for five different droplets at different locations on devices. To ensure IJP devices were similar from device to device, DC trials were repeated on four separate devices.

Electrowetting performance was similar between devices for DC actuation (Fig. 4.7a). The cosine of the apparent contact angle is plotted as a function of the electrowetting number to account for variability between devices. Behavior was well predicted through the electrowetting equation. The average electrowetting number and initial apparent contact angle between IJP devices was used to predict the trend in the electrowetting equation. Predictions for devices were well predicted up to $Ew \approx 1$ or $V \approx 120V$, when contact angle saturation occurs. It should be noted the difference between IJP and CRF devices for DC actuation trials was due to the IJP devices having a thinner

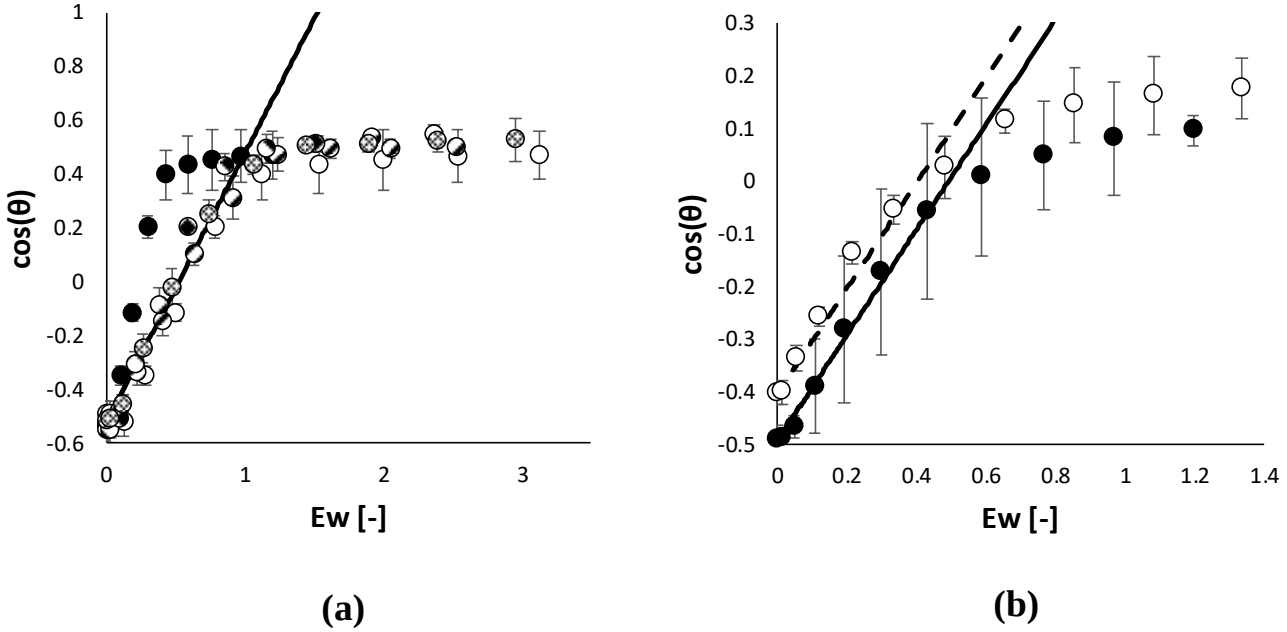

Figure 4.7 Experimentally observed cosine of apparent contact angles on CRF (closed) and IJP (open/patterned) devices as a function of electrowetting number for applied DC (a) and AC (b) voltages. Predictions from the Electrowetting Equation are represented by solid and dashed lines.

SU-8 layer. The smaller thickness is due to the layer of Teflon between the electrode and SU-8. This layer thickness difference also resulted in a higher Ew value for the IJP devices used in the DC trials.

The difference between CRF and IJP devices for the AC case is largely due a difference in initial contact angle (Fig. 4.7b). The CRF and IJP devices had an initial contact angle of 118.5^o and 113.8^o respectively. It was observed the initial contact angles between IJP devices varied more greatly compared to CRF devices. Despite this variation, both devices were well predicted through the electrowetting equation. The large value of uncertainty of the IJP device could be attributed to a not flat surface due to the baking process after spin coating. As the applied AC voltage increased, the droplets began to move around on the slide. As a result, the apparent contact angle measurements varied.

The similarity in apparent contact angles and electrowetting performance between devices does not ensure the contact angle hysteresis will be similar [44]. Applications concerning colloidal deposition are affected heavily by contact angle hysteresis. The depinning of the contact line can have a dramatic effect in the flow of an evaporating droplet [22, 44, 57]. Therefore, the second set of experiments analyzed variability of contact angle hysteresis between devices. These experiments were performed prior to the purchase of the Ramè-Hart Automated Dispensing System. A micrometer syringe was used to manually add and remove fluid at a constant rate while being actuated at a constant voltage. Droplets were actuated at voltages ranging from $0 - 120V_{RMS}$ in $20V$ increments. This set of experiments only focused on using AC actuation.

Contact angle hysteresis is similar between devices (Fig. 4.8) agreeing within $0.2° \pm 3.0°$ across all electrowetting numbers examined. Like the previous experiment, there is a variation between IJP and CRF devices due to varying initial contact angles. Both devices follow the predicted trend described through Eq. 1.10 and 4.2 for the cosine of advancing and receding values (respectively).

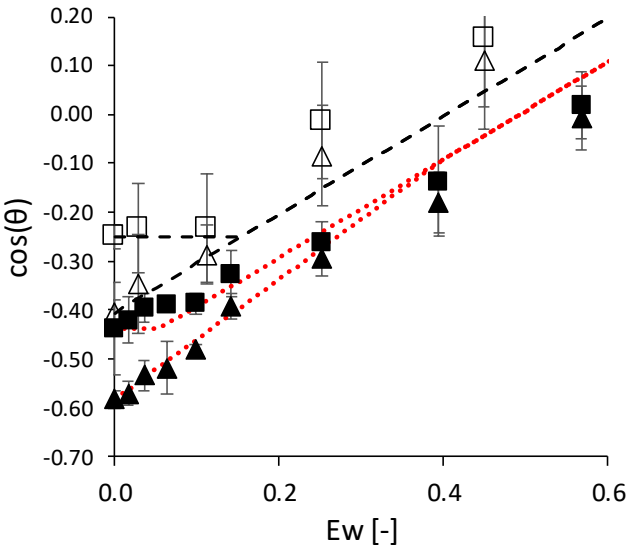

Figure 4.8 Experimentally observed hysteresis data for CRF (closed) and IJP (open) devices as a function of electrowetting number for the cosine of advancing (triangle) and receding (square) angles. Predictions from Eq. 1.10 and 4.2 are displayed for IJP (black dash) and CRF (red dotted) devices.

The IJP values are anticipated to have a larger level of uncertainty of advancing and receding angles due to the larger variation in surface inhomogeneities. It can clearly be seen the level of uncertainty for IJPs is much higher than the CRFs. This implies the CRF device is more accurate.

Increased roughness of the IJP electrodes could also increase apparent heterogeneity of the device under an applied voltage due to variations in the local electrowetting number (Fig. 4.9a,b) [58]. If the roughness of the conductive layer was significant relative to the dielectric layer thickness, areas with thinner dielectric layers would increase Ew and decrease Ew in areas with thicker dielectric layers (Fig. 4.9c). It would be expected for the apparent heterogeneity to increase at low-to-moderate voltages when there are appreciable differences in dielectric layer thickness.

Similarly, it would be expected to decrease at larger voltages as local apparent contact angles become saturated (Fig. 4.9d). The increased uncertainty of initial apparent contact angles supports the hypothesis the roughness of the printed electrodes increases the heterogeneity of the surface of the device due to increasing the density of surface defects.

Based off empirical data, IJP devices can be substituted for CRF devices. Due to device repeatability and lower surface inhomogeneities, CRF devices are superior to IJP devices. The production of IJP devices leads to a larger level of uncertainty within experimental data. This suggests that further experimentation and analysis is required for these devices.

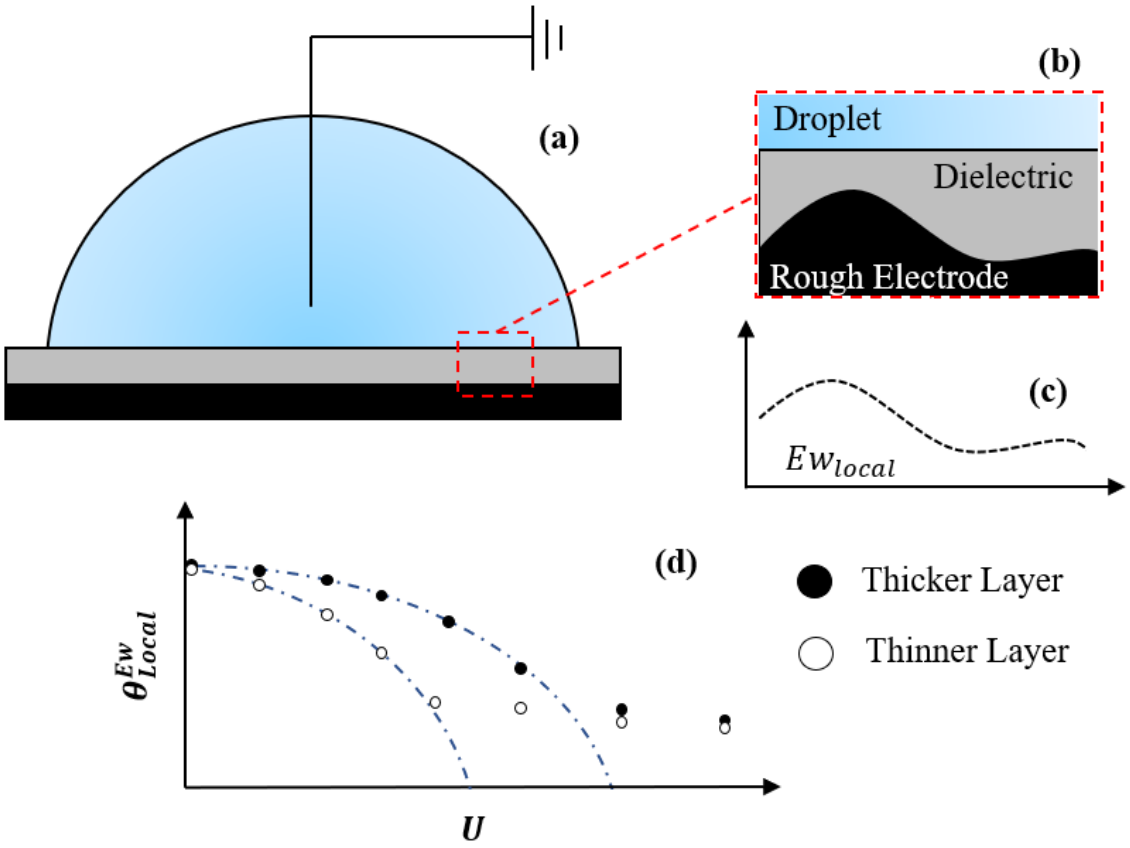

Figure 4.9 Side-view sketch of a DMF device (a), an exploded view showing the difference in electrode roughness (not to scale) (b), and expected effects of differences in local dielectric layer thickness on electrowetting number (c) and electrowetting performance (d).

4.4 Effects of Particle Concentration

The effect nanoparticles have on the hysteresis of an actuated droplet was analyzed. Microfluidic devices used within this section were unpatterned electrodes with SU-8 3005 as the dielectric layer and Teflon as the hydrophobic layer. Droplets used $22nm$ polystyrene (PS) particles in concentrations of 0.01% and 0.001%. Hysteresis data collected from the Teflon device in Section 4.2 was used as the control case for comparison. Experimentation followed similar procedures as the previous two sections.

Droplets containing any concentration of particles exhibited an agreement in predictions for both the electrowetting equation and the model used to predict the hysteresis for a droplet with no concentration (Fig. 4.10 and 4.11). Both cases are well predicted by the electrowetting and hysteresis equations. This implies the PS nanoparticles do not effect the contact line when receding

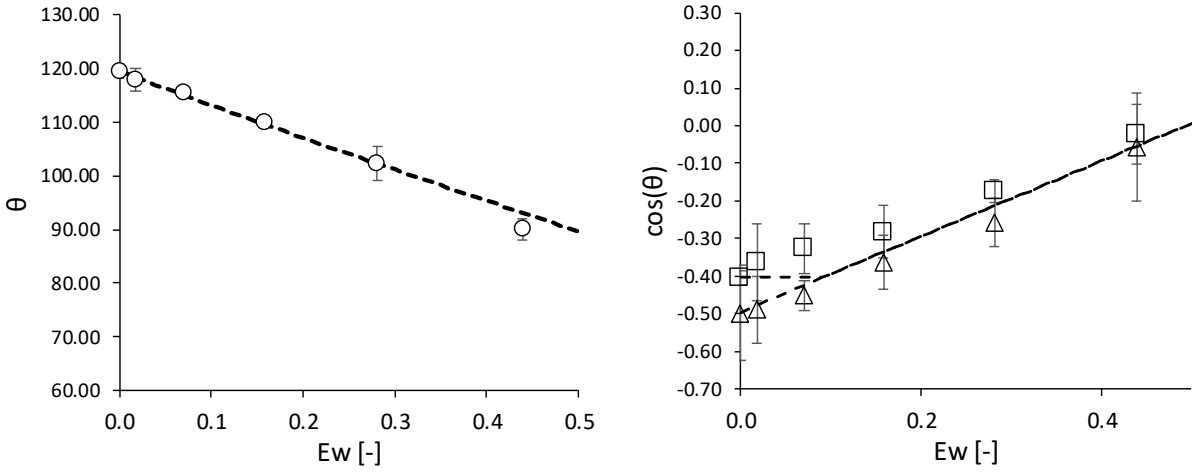

Figure 4.10 Experimentally observed electrowetting data for droplets with 0.001% concentration of PS particles as a function of electrowetting number (a) and the cosine of advancing (triangle) and receding (square) angles (b).

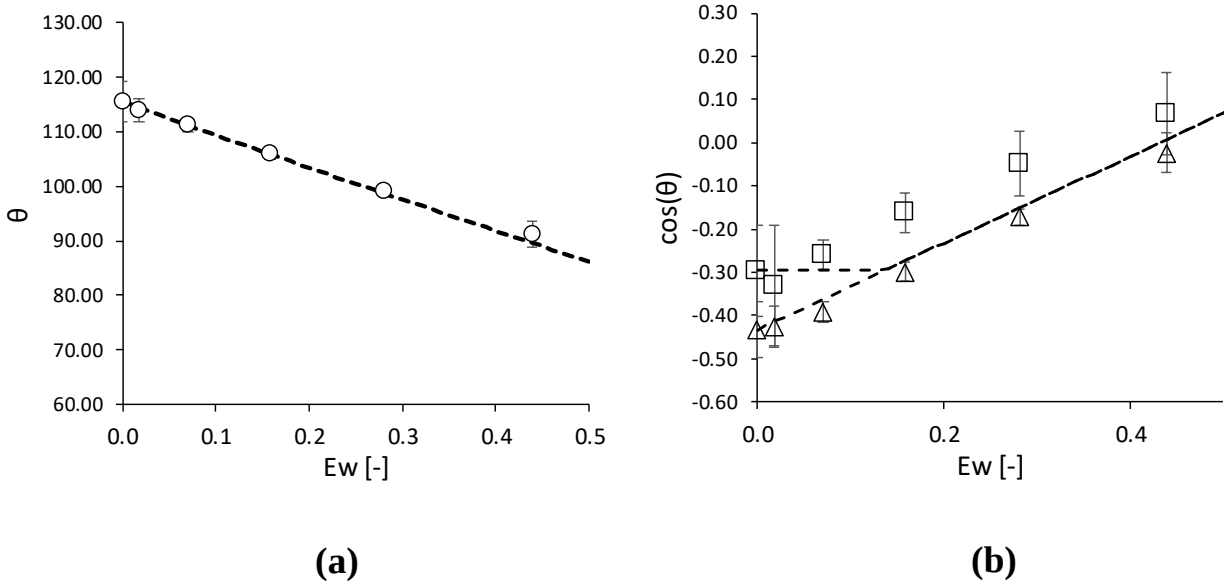

Figure 4.11 Experimentally observed electrowetting data for droplets with 0.01% concentration of PS particles as a function of electrowetting number (a) and the cosine of advancing (triangle) and receding (square) angles (b).

or advancing.

While the experimental data agrees with the models for droplets with PS particles, this does not necessarily mean all scenarios with particles will act similarly. The concentration, size, and type of particle could alter these results and further experimentation is required to fully understand all potential scenarios. Literature suggests the addition of particles promotes slip-stick behavior [49]. It is possible other scenarios during actuation may demonstrate slip-stick behavior. If the particles do affect the motion of the contact line, there are two hypotheses proposed to explain the phenomenon. Both hypotheses proposed will require further experimentation.

When a droplet is placed on a substrate, the contact line experiences some displacement prior to reaching equilibrium (Fig. 4.12). After the droplet is deposited (Fig. 4.12a), the contact line increases, thus decreasing the contact angle (Fig. 4.12b). Following the increase in contact

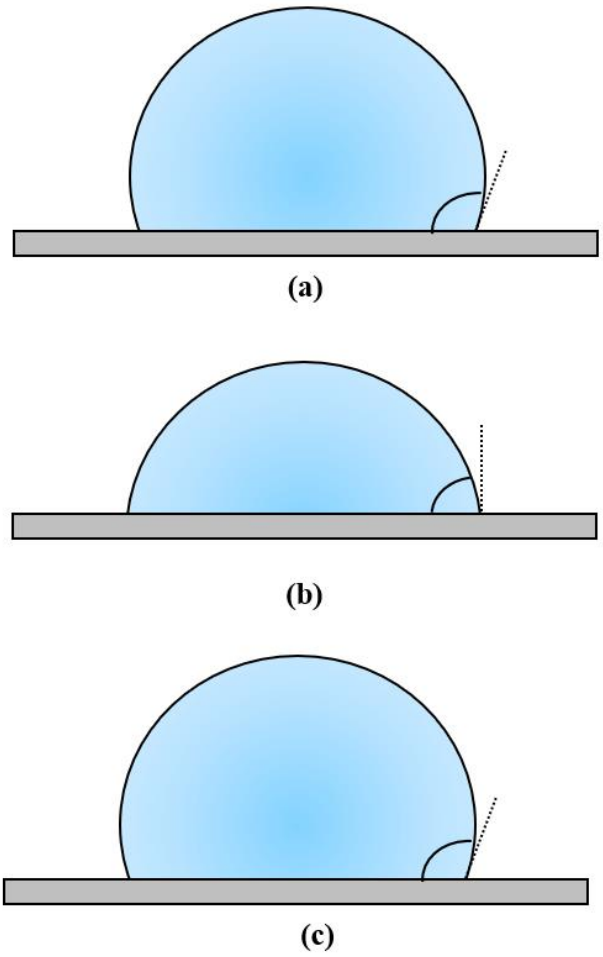

Figure 4.12 Phases of the contact angle as a droplet is placed on a substrate.

line, the pinning forces move the contact line back in, increasing the contact angle (Fig. 4.12c). This phenomenon was observed on a DI droplet using a highspeed camera at $600\ fps$. Otherwise the movement of the contact line happens so quickly it is not able to be seen by the human eye. Droplets when actuated were also observed to experience this phenomenon.

It is hypothesized that when a droplet with particles is placed on a substrate, the particles prevent the contact line to reach the equilibrium angle expected in a particle free droplet. As a result, the particles prevent a droplet to recede to its full potential (Fig. 4.13c). These findings agree with what was found in literature for unactuated evaporating droplets [16]. A larger force is

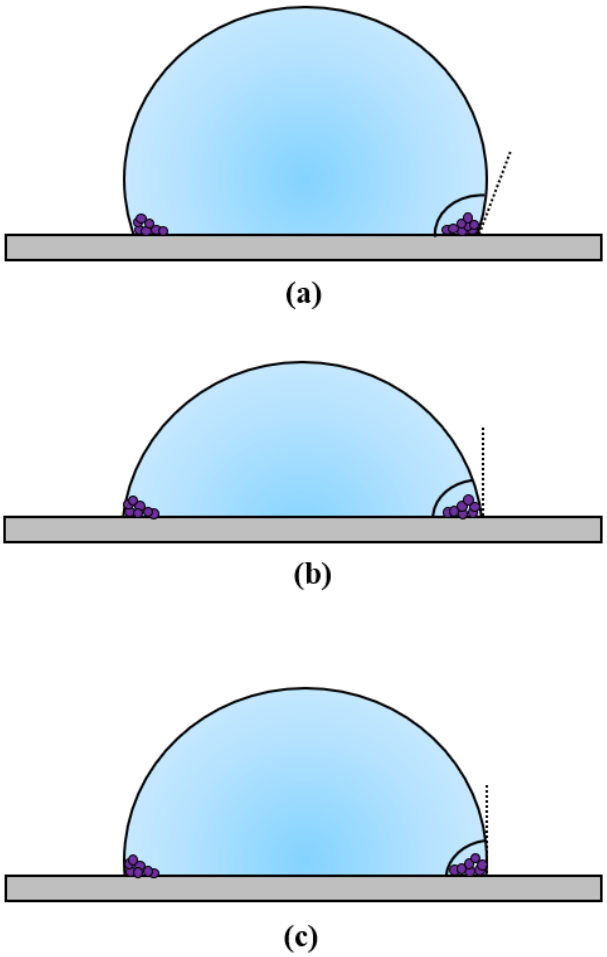

Figure 4.13 Phases of the contact angle as a droplet with particles is placed on a substrate (particles not to scale).

required to overcome the particles. Therefore, the higher the particle concentration is within a droplet, the larger the force will need to be. This work is all preliminary and requires further experimentation to test and verify this hypothesis. Experimentation would include use of a highspeed camera to visually understand what is happening as the droplet is moving.

The second hypothesis suggests the clumping of particles at the contact line could be affecting the electric field. It is possible the electric field is travelling through the polystyrene particles. Polystyrene is a known insulator and therefore can inhibit the flow of electricity through the droplet. This would lead to the need for a higher electric field as the particle concentration

increases. Further testing is required to determine if this hypothesis is correct. Experimentation would require tests using a variety of different particle types and concentrations. Particles should vary in permittivity to determine if there is a correlation between conductivity and its effect on the contact line. The work performed in this thesis using particles is all preliminary work and requires extensive testing to fully understand this phenomenon.

5.0 CONCLUSIONS

5.1 Summary

This work investigates the different factors that could affect contact line pinning when electrowetting on dielectric. The four factors investigated within this thesis were effect electrowetting has on contact line pinning, top surface layers on the dielectric, electrode manufacturing process, and particle concentration of droplets. To accomplish the goals of this work, two separate experiments were designed to characterize the effects of these factors. The first experiment analyzed how well the electrowetting equation predicts a droplet's contact angle on a surface. The second experiment characterized the contact angle hysteresis which could be used to quantify the contact line pinning forces acting on a droplet. The level of uncertainty within this investigation could potentially be accounted for due to the surface roughness of the devices.

Experimental data on various surfaces suggests the model presented in literature [27] to characterize the advancing and receding contact angles could be improved. The model presented within literature was moderately accurate for devices that used Teflon as the hydrophobic layer. When the hydrophobic layer of the device was not Teflon, the model did not effectively quantify the pinning forces. An updated model was proposed to more accurately describe the transient forces that were affecting the contact line when advancing. While literature quantified these forces by using the maximum value of Eq. 4.1, this work proposed to use the RMS value. Using the RMS value is hypothesized to more accurately capture the transient nature of the term. This implies the contact line motion is not dominated by the instantaneous maximum. This assumption is similar to using the RMS voltage when electrowetting.

The updated model is 20%, 60%, and 55% more accurate for low to moderate voltages on

Teflon, PDMS, and SU-8 (respectively). Like the electrowetting equation, this model is valid until the droplet reaches a saturation point. The total dimensionless pinning force once reaching saturation were relatively similar, never reaching zero. This suggests the total dimensionless pinning force could never equal zero as literature suggests [27] and the saturated pinning force is affected by some factor. This factor is hypothesized to be the material properties of the top layer of the microfluidic device.

Additionally, the manufacturing process of the electrode may influence the contact line pinning forces when EWOD. Experimentation tested to determine if IJP devices could be characterized by the electrowetting equation (Eq. 1.1) and the hysteresis model. It was found IJP devices are a viable substitute for CRF devices; however, CRF devices are more accurate. Further testing and experimentation are required to reduce the level of uncertainty of IJP devices.

Actuated droplets with various concentrations of $22nm$ PS particles was analyzed. Droplets with particles were well predicted by the electrowetting equation and the updated hysteresis model. Experimental data suggests droplets with particles does not affect the motion of the contact line. Literature suggests the opposite [49], therefore further analysis of droplets under a variety of scenarios is required to determine if this is true for all cases. If this is untrue for all cases, additional testing of droplets under a highspeed camera is required to understand what is occurring instantaneously to the droplet when: it is actuated, advancing, and receding. This additional experimentation would also serve to determine if the particles are affecting the electric field. This would be done by using various types and concentrations of particles with different electrical properties.

5.2 Contributions

This work has increased the understanding of the contact line forces that affect a droplet when electrowetting on dielectric. An updated and more accurate model to predict the advancing angle for a droplet for relatively low to moderate voltages was developed. This model was also improved to predict when the advancing and receding angles would converge. This updated model increases the ability to predict when a droplet will reach its lowest hysteresis value. As well as the amount of voltage required to reach that value. This model was determined to be valid for a variety of surfaces that have different properties such as: hydrophobic, hydrophilic, low hysteresis, and high hysteresis.

Device fabrication methods were also analyzed within this work. A more economic means of electrode fabrication was developed within this investigation. Using an Epson Stylus C88+ Inkjet Printer eliminates the need of a cleanroom facility. Removing the need for a cleanroom reduces the fabrication time and cost tremendously. The devices tested in this work were found to be a suitable replacement for CRF devices. These efforts were to meet ASSURED criteria for digital microfluidic devices. They are also a suitable for rapid test prototyping for various digital microfluidic designs.

The final phase of this work analyzed the effect particles have on an actuated droplet. Literature presented the contact line motion exhibits slip stick behavior when particles are present in an evaporating droplet. This investigation found the contact angles of droplets with particles are overpredicted through the electrowetting equation and hysteresis model. Further investigation is required to further understand this phenomenon. However, this is the first step towards improving sepsis detection using digital microfluidic devices.

The work presented in this thesis has already been submitted and accepted to various

journals. The work presented in Section 4.2 is being prepared for submission and is expected to be ready for submission by May 2019. The following works already published include the following:

1) K.A. Bernetski, C.T. Burkhart, K.L. Maki, M.J. Schertzer, Characterization of electrowetting, contact angle hysteresis, and adhesion on digital microfluidic devices with inkjet-printed electrodes, Microfluid. Nanofluidics. 22 (2018) 1–10. doi:10.1007/s10404-018-2119-4.
2) K.A. Bernetski, K.L. Maki, M.J. Schertzer, Comment on "How to make sticky surfaces slippery: Contact angle hysteresis in electrowetting with alternating voltage" [Appl. Phys. Lett. **92** , 244108 (2008)], Appl. Phys. Lett. 114 (2019) 116101. doi:10.1063/1.5080091.

The following work is also in preparation:

3) K.A. Bernetski, K.L. Maki, M.J. Schertzer, (In preparation) A model for contact angle hysteresis under AC Electrowetting on a variety of surfaces.

All necessary data for the initial submission of this paper is presented hereand submission to Applied Physics Letters is expected by May 2019.

5.3 Future Work

Some of the work presented in this thesis requires further experimentation. Additional analysis is required to further understand the results in Section 4.4. The first step would require testing various particle types, sizes, and concentrations. If there is deviation of this model for any scenario, there are two proposed hypotheses that could be tested to understand the phenomenon. Analysis of the first proposed hypothesis in Section 4.4 could be tested by running similar hysteresis experiments using a higher speed camera. Using a higher speed camera would allow better visualization of what is happening to the droplet at any instantaneous moment. It has been

seen in preliminary work the contact line of a particle free droplet fluctuates a small amount while it is actuated with an AC current. Analysis with a high-speed camera would allow observation of this phenomenon occurring on droplets with particles. Additionally, similar experiments from [49] could be performed on actuated evaporating droplets. Unlike literature, this analysis would apply an AC voltage to droplets at varying voltages to quantify the effects of an electric field.

The second proposed hypothesis in Section 4.4 could be tested by running similar hysteresis experiments using various concentrations of particles that vary in permittivity. Polystyrene is a known insulator. Therefore, it is hypothesized the particles were inhibiting the electric field in the droplet. Using particles that would cover a spectrum of insulators and conductors would test to see how the permittivity of the particles affect the contact line motion of a droplet.

REFERENCES

[1] J. Cohen, “The immunopathogenesis of sepsis,” *Nature*, vol. 420, no. 6917, pp. 885–891, 2002.

[2] D. C. Angus, W. T. Linde-zwirble, J. Lidicker, G. Clermont, J. Carcillo, and M. R. Pinsky, “Epidemiology of severe sepsis in the United States: Analysis of incidence, outcome, and associated costs of care,” vol. 29, no. 7, pp. 1303–1310, 2001.

[3] “Label Free Sepsis Detection via Manipulation of Colloidal Transport and Deposition in Evaporating Droplets : A Multidisciplinary Approach A . Project Goal and Objectives of the Proposed Work,” no. 1, pp. 1–15.

[4] J. Hellman *et al.*, “Antiserum against Escherichia coli J5 Contains Antibodies Reactive with Outer Membrane Proteins of Heterologous Gram-Negative Bacteria,” no. April, pp. 1260–1268, 2018.

[5] J. Hellman *et al.*, “Outer Membrane Protein A , Peptidoglycan-Associated Lipoprotein , and Murein Lipoprotein Are Released by Escherichia coli Bacteria into Serum,” vol. 68, no. 5, pp. 2566–2572, 2000.

[6] G. McHale, “Surface free energy and microarray deposition technology,” *Analyst*, vol. 132, no. 3, pp. 192–195, 2007.

[7] V. Ragoonanan and A. Aksan, “Heterogeneity in desiccated solutions: Implications for biostabilization,” *Biophys. J.*, vol. 94, no. 6, pp. 2212–2227, 2008.

[8] C. P. Gulka *et al.*, “Coffee rings as low-resource diagnostics: Detection of the malaria biomarker plasmodium falciparum histidine-rich protein-II using a surface-coupled ring of Ni(II)NTA gold-plated polystyrene particles,” *ACS Appl. Mater. Interfaces*, vol. 6, no. 9,

pp. 6257–6263, 2014.

[9] J. R. Trantum, D. W. Wright, and F. R. Haselton, “Biomarker-mediated disruption of coffee-ring formation as a low resource diagnostic indicator,” *Langmuir*, vol. 28, no. 4, pp. 2187–2193, 2012.

[10] C. T. Burkhart, U. States, K. L. Maki, U. States, and M. J. Schertzer, “ICNMM2016-7988 OBSERVATION OF CONTACT LINE DYNAMICS IN EVAPORATING DROPLETS,” in *ASME International Conference on Nanochannels, Microchannels, and Minichannels*, 2017, pp. 1–6.

[11] R. W. Peeling, K. K. Holmes, D. Mabey, and A. Ronald, “Rapid tests for sexually transmitted infections (STIs): the way forward,” *Sex. Transm. Infect.*, vol. 82, no. suppl_5, pp. v1–v6, 2006.

[12] M. L. Y. Sin, J. Gao, J. C. Liao, and P. K. Wong, “System Integration - A Major Step toward Lab on a Chip System Integration - A Major Step toward Lab on a Chip,” vol. 6, no. May, 2011.

[13] G. Mchale, “Surface free energy and microarray deposition technology,” vol. 44, no. 0, pp. 1–3, 2007.

[14] M. Layani, M. Gruchko, O. Milo, I. Balberg, D. Azulay, and S. Magdassi, “Transparent conductive coatings by printing coffee ring arrays obtained at room temperature,” *ACS Nano*, vol. 3, no. 11, pp. 3537–3542, 2009.

[15] V. A. Online, V. Bromberg, F. D. Egitto, and T. J. Singler, “of inkjet-printed silver nitrate traces,” pp. 6842–6849, 2013.

[16] D. Orejon, K. Se, and M. E. R. Shanahan, “Stick À Slip of Evaporating Droplets : Substrate Hydrophobicity and Nanoparticle Concentration,” pp. 12834–12843, 2011.

[17] Y. Chen, J. D. Müller, P. T. C. So, and E. Gratton, “The photon counting histogram in fluorescence fluctuation spectroscopy,” *Biophys. J.*, vol. 77, no. 1, pp. 553–567, 1999.

[18] E. Bellido *et al.*, “Controlled positioning of nanoparticles on graphene by noninvasive AFM lithography,” *Langmuir*, vol. 28, no. 33, pp. 12400–12409, 2012.

[19] G. Corkidi, F. Montoya, G. H. Cruz, and M. Vargas, “Evaporation dynamics and sedimentation pattern of a sessile particle laden water droplet,” *Exp. Fluids*, vol. 57, no. 6, pp. 1–11, 2016.

[20] A. Saha, S. Basu, and R. Kumar, “Particle image velocimetry and infrared thermography in a levitated droplet with nanosilica suspensions,” *Exp. Fluids*, vol. 52, no. 3, pp. 795–807, 2012.

[21] J. Park and J. Moon, “Control of colloidal particle deposit patterns within picoliter droplets ejected by ink-jet printing,” *Langmuir*, vol. 22, no. 8, pp. 3506–3513, 2006.

[22] R. G. Larson, “Transport and Deposition Patterns in Drying Sessile Droplets,” vol. 60, no. 5, 2014.

[23] H. B. Eral, D. M. Augustine, M. H. G. Duits, and F. Mugele, “Suppressing the coffee stain effect: how to control colloidal self-assembly in evaporating drops using electrowetting,” *Soft Matter*, vol. 7, no. 10, p. 4954, 2011.

[24] D. Mampallil, H. B. Eral, D. Van Den Ende, and F. Mugele, “Control of evaporating complex fluids through electrowetting,” *Soft Matter*, vol. 8, no. 41, pp. 10614–10617, 2012.

[25] D. Orejon, K. Sefiane, and M. E. R. Shanahan, “Edinburgh Research Explorer Evaporation of nanofluid droplets with applied DC potential,” *J. Colloid Interface Sci.*, vol. 407, pp. 29–38, 2013.

[26] F. Li and F. Mugele, “How to make sticky surfaces slippery : Contact angle hysteresis in electrowetting with alternating voltage How to make sticky surfaces slippery : Contact angle hysteresis in electrowetting with alternating voltage,” vol. 244108, no. 2008, pp. 2006–2009, 2011.

[27] F. Li and F. Mugele, “How to make sticky surfaces slippery: Contact angle hysteresis in electrowetting with alternating voltage,” *Appl. Phys. Lett.*, vol. 92, no. 24, pp. 2006–2009, 2008.

[28] C. T. Burkhart and C. T. Burkhart, “Characterizing the Transient Profile Shapes and Deposition Patterns of Desiccating Colloidal Droplets Characterizing the Transient Profile Shapes and Deposition Patterns of Desiccating Colloidal Droplets,” 2016.

[29] T. Coltro, C. Cheng, E. Carrilho, and D. P. De Jesus, “Recent advances in low-cost microfluidic,” pp. 2309–2324, 2014.

[30] C. Dixon, A. H. C. Ng, R. Fobel, M. B. Miltenburg, and A. R. Wheeler, “An inkjet printed, roll-coated digital microfluidic device for inexpensive, miniaturized diagnostic assays,” *Lab Chip*, vol. 16, no. 23, pp. 4560–4568, 2016.

[31] R. D. Deegan, O. Bakajin, and T. F. Dupont, “Capillary flow as the cause of ring stains from dried liquid drops,” pp. 827–829, 1997.

[32] R. D. Deegan, “Pattern formation in drying drops,” *Phys. Rev. E - Stat. Physics, Plasmas, Fluids, Relat. Interdiscip. Top.*, vol. 61, no. 1, pp. 475–485, 2000.

[33] Æ. Je, “Dynamics of droplet transport induced by electrowetting actuation,” pp. 287–294, 2008.

[34] J. Lee, H. Moon, J. Fowler, T. Schoellhammer, and C. J. Kim, “Electrowetting and electrowetting-on-dielectric for microscale liquid handling,” *Sensors Actuators, A Phys.*,

vol. 95, no. 2–3, pp. 259–268, 2002.

[35] S. K. Cho, H. Moon, and C.-J. Kim, “Creating, transporting, cutting, and merging liquid droplets by electrowetting-based actuation for digital microfluidic circuits,” *J. Microelectromechanical Syst.*, vol. 12, no. 1, pp. 70–80, 2003.

[36] K. H. Kang, “How electrostatic fields change contact angle in electrowetting,” *Langmuir*, vol. 18, no. 26, pp. 10318–10322, 2002.

[37] M. J. Schertzer, S. I. Gubarenko, R. Ben-Mrad, and P. E. Sullivan, “An empirically validated analytical model of droplet dynamics in electrowetting on dielectric devices,” *Langmuir*, vol. 26, no. 24, pp. 19230–19238, 2010.

[38] P. Paik, V. K. Pamula, M. G. Pollack, and R. B. Fair, “Electrowetting-based droplet mixers for microfluidic systems.,” *Lab Chip*, vol. 3, no. 1, pp. 28–33, Feb. 2003.

[39] R. Bhardwaj, X. Fang, P. Somasundaran, and D. Attinger, “Self-assembly of colloidal particles from evaporating droplets: Role of DLVO interactions and proposition of a phase diagram,” *Langmuir*, vol. 26, no. 11, pp. 7833–7842, 2010.

[40] C. Hurth *et al.*, “Biomolecular interactions control the shape of stains from drying droplets of complex fluids,” *Chem. Eng. Sci.*, vol. 137, pp. 398–403, 2015.

[41] H. Hu and R. G. Larson, “Evaporation of a sessile droplet on a substrate,” *J. Phys. Chem. B*, vol. 106, no. 6, pp. 1334–1344, 2002.

[42] R. D. Deegan, O. Bakajin, T. F. Dupont, G. Huber, S. R. Nagel, and T. A. Witten, “Contact Line Deposits in an Evaporating Drop,” no. August 2000, 2014.

[43] H. Hu and R. G. Larson, “Marangoni effect reverses coffee-ring depositions,” *J. Phys. Chem. B*, vol. 110, no. 14, pp. 7090–7094, 2006.

[44] C. T. Burkhart, K. L. Maki, and M. J. Schertzer, “Effects of Interface Velocity, Diffusion

Rate, and Radial Velocity on Colloidal Deposition Patterns Left by Evaporating Droplets," *J. Heat Transfer*, vol. 139, no. 11, p. 111505, 2017.

[45] Y. D. Shikhmurzaev, "On Young ' s (1805) equation and Finn ' s (2006) ' counterexample ,'" vol. 372, pp. 704–707, 2008.

[46] F. Mugele and J.-C. Baret, "Electrowetting: from basics to applications," *J. Phys. Condens. Matter*, vol. 17, no. 28, pp. R705–R774, 2005.

[47] L. Chen and E. Bonaccurso, "Electrowetting - From statics to dynamics," *Adv. Colloid Interface Sci.*, vol. 210, pp. 2–12, 2014.

[48] E. Schäffer, "Dynamics of Contact Line Pinning in Capillary Rise and Fall," no. September, 2015.

[49] D. Orejon, K. Sefiane, and M. E. R. Shanahan, "Stick-slip of evaporating droplets: Substrate hydrophobicity and nanoparticle concentration," *Langmuir*, vol. 27, no. 21, pp. 12834–12843, 2011.

[50] "Cyanoresin Brochure.Pdf." .

[51] P. Epoxy and N. Photoresist, "SU-8 3000 Permanent Epoxy," vol. 20, 2000.

[52] S. D. Sheet, "SIGMA-ALDRICH," 2018.

[53] K. A. Bernetski, K. L. Maki, and M. J. Schertzer, "Comment on 'How to make sticky surfaces slippery: Contact angle hysteresis in electrowetting with alternating voltage' [Appl. Phys. Lett. **92** , 244108 (2008)]," *Appl. Phys. Lett.*, vol. 114, no. 11, p. 116101, 2019.

[54] D. Mampallil and H. Burak, "A review on suppression and utilization of the coffee-ring effect," *Adv. Colloid Interface Sci.*, vol. 252, pp. 38–54, 2018.

[55] W. C. Nelson and C.-J. 'Cj' Kim, "Droplet Actuation by Electrowetting-on-Dielectric

(EWOD): A Review," *J. Adhes. Sci. Technol.*, vol. 26, no. 12–17, pp. 1747–1771, 2012.

[56] R.V. Sedev, J.G. Petrov, and A. W. Neumann, "Effect of Swelling of a Polymer Surface on Advancing and Receding Contact Angles," *J. Colloid Interface Sci.*, vol. 180, pp. 36–42, 1996.

[57] H. Masoud and J. D. Felske, "Analytical solution for Stokes flow inside an evaporating sessile drop: Spherical and cylindrical cap shapes," *Phys. Fluids*, vol. 21, no. 4, pp. 1–33, 2009.

[58] K. A. Bernetski, C. T. Burkhart, K. L. Maki, and M. J. Schertzer, "Characterization of electrowetting, contact angle hysteresis, and adhesion on digital microfluidic devices with inkjet-printed electrodes," *Microfluid. Nanofluidics*, vol. 22, no. 9, pp. 1–10, 2018.